Underground Injection Control – Class VI Permit Application for Mockingbird Carbon Storage Project Injection Wells No. 01, No. 02, No. 03, and No. 04

SECTION 1 – SITE CHARACTERIZATION

Mockingbird Carbon Storage Project
Allen Parish, Louisiana
ExxonMobil Low Carbon Solutions Onshore Storage, LLC
April 2025

SECTION 1 – SITE CHARACTERIZATION

TABLE OF CONTENTS

Figures

[redacted]

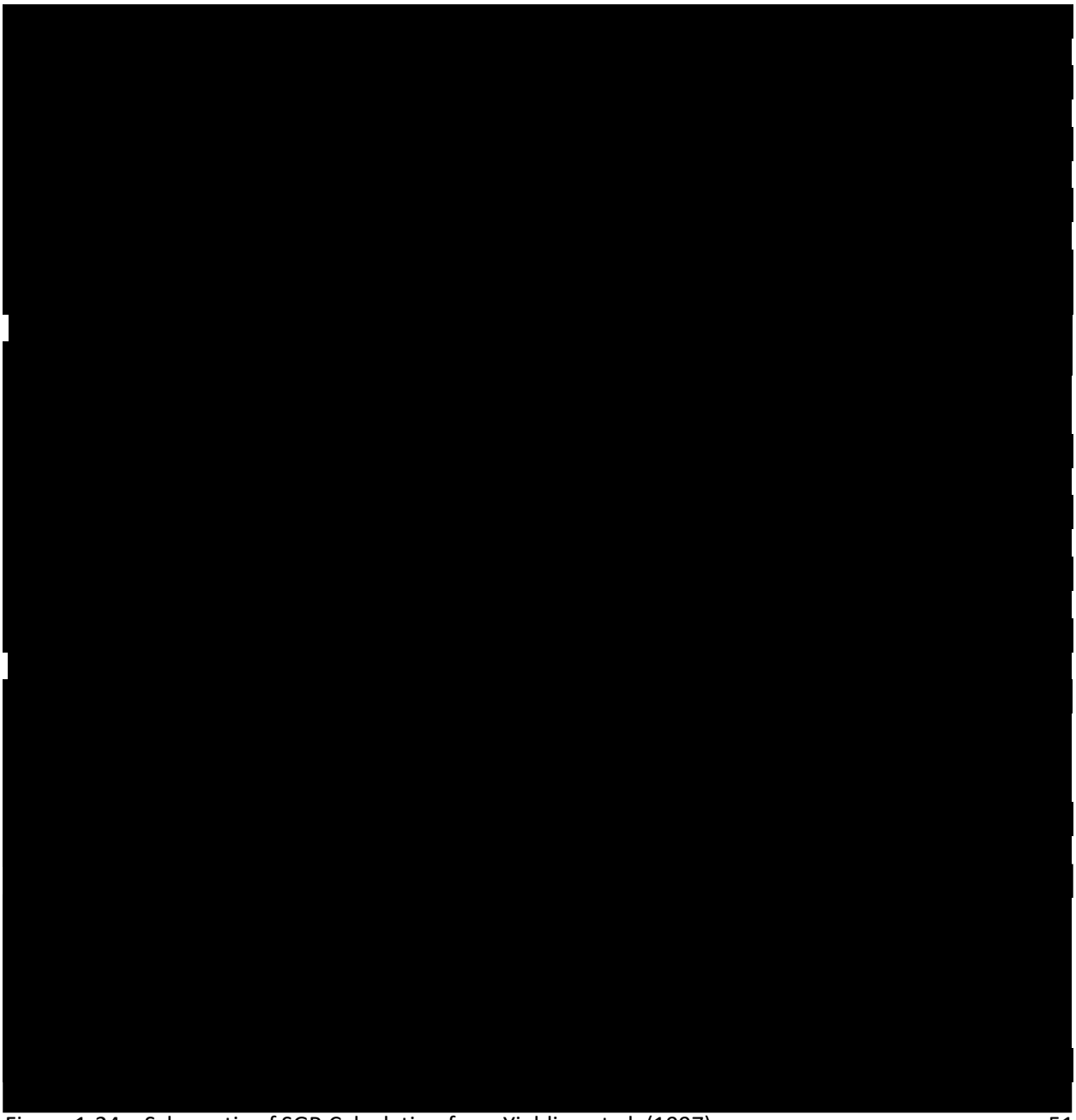

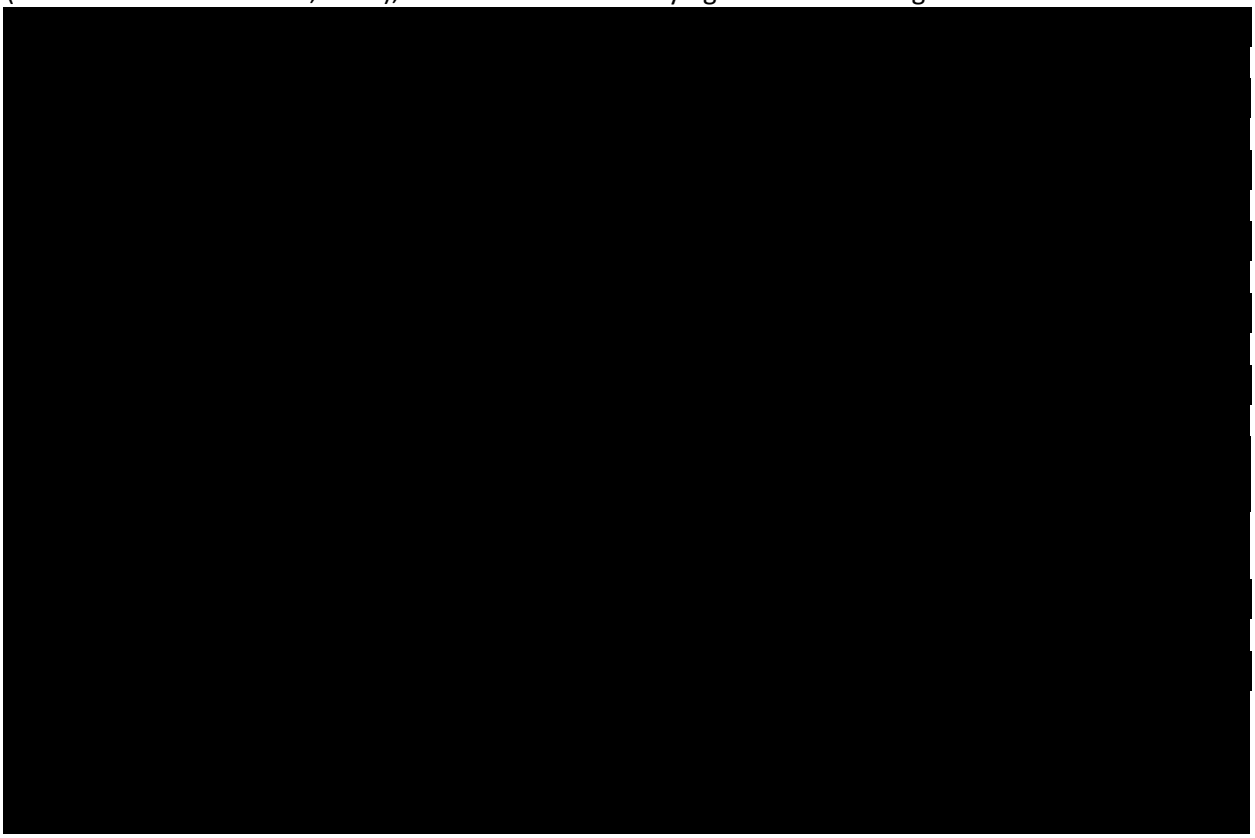

Tables

1.1 Overview

The site characterization for the proposed Mockingbird Carbon Storage (CS) (Mockingbird) Project was prepared to meet the requirements of Louisiana Administrative Code, Title 43 (LAC43): XVII **§3607.C.1.b**. ExxonMobil Low Carbon Solutions Onshore Storage, LLC (ExxonMobil) is undertaking the project in Allen Parish, Louisiana, [redacted] The purpose of this site characterization is to identify the potential risks and demonstrate, to the satisfaction of the Commissioner of Conservation (Commissioner), that the proposed site is suitable for the sequestration project. The key aspects of this demonstration are that the geologic formations provide adequate storage capacity to store the intended volume of injected CO_2, and that a competent confining zone is present that will contain the injected CO_2 throughout the life of the project.

ExxonMobil has completed a review of site characterization data and analyses from multiple data types including public, proprietary, and licensed data sets. A high degree of confidence has been gained during this process regarding the effectiveness of the storage and confining properties of the sequestration site, and the anticipated alignment with data that will become available in the future.

1.1.1 Objectives

The following objectives were developed to demonstrate compliance with the requirements of LAC43: XVII **§3607**:

- Provide maps and cross sections of the area of review (AOR) (LAC43: XVII **§3607.C.1.b.ii** and **§3607.C.1.a**).
- Summarize available data on the depth, areal extent, thickness, mineralogy, porosity, permeability, and capillary pressure of the injection and confining zones and on lithology and facies changes (LAC43: XVII **§3607.C.2.a**).
- Provide geologic and topographic maps and cross sections illustrating regional geology, hydrogeology, and the geologic structure of the local area (LAC43: XVII **§3607.C.1.b.i**).
- Identify the location, orientation, and properties of known or suspected faults and fractures that may transect the confining zones in the AOR, along with an assessment that the faults/fractures will not interfere with containment (LAC43: XVII **§3607.C.1.b.iii**).
- Discuss the available geomechanical information on fractures, stress, ductility, rock strength, and in situ fluid pressures within the confining zones (LAC43: XVII **§3607.C.2.b**).
- Present maps and stratigraphic cross sections indicating the general vertical and lateral limits of the underground sources of drinking water (USDWs) and water well completion details within the AOR, their positions relative to the injection zone, and the direction of water movement (where known) (LAC43: XVII **§3607.C.2.b.iv**).
- Summarize the available baseline geochemical data on subsurface formations, including the USDWs in the AOR (LAC43: XVII **§3607.C.2.e**).

- Summarize the available information on the seismic history of the area, including the presence and depths of seismic sources, and an assessment of the potential for seismicity to interfere with containment (LAC43: XVII **§3607.C.2.c**).

1.2 Regional Geology

Tectonostratigraphic and Paleoclimatic History – Northern Portion of the Gulf of Mexico Basin

The incipient Gulf of Mexico basin (Figure 1-1) formed through the extension of largely continental crust during the Late Triassic to Early Jurassic breakup of the Pangean supercontinent, specifically rifting between the North American and South American plates (Bird et al., 2005 and references therein; Galloway, 2008). Rifting and basin growth accelerated into the Late Jurassic and Early Cretaceous (Salvador, 1987; Jacques and Clegg, 2002; Galloway, 2008). As a result, areas immediately outside the basin consist of unmodified continental crust, while the basin itself is underlain by shallow (2–12 kilometers deep), moderately thinned, transitional crust along the margin—and progressively more extended, thinner, and deeper (up to 20 kilometers) transitional crust to marine crust near the basin center (Galloway, 2008). Crustal extension prior to this accelerated growth phase ultimately resulted in a structural sag on the western side of the basin.

All figures here in *Section 1.2* are displayed in high resolution in *Appendix B-1***.**

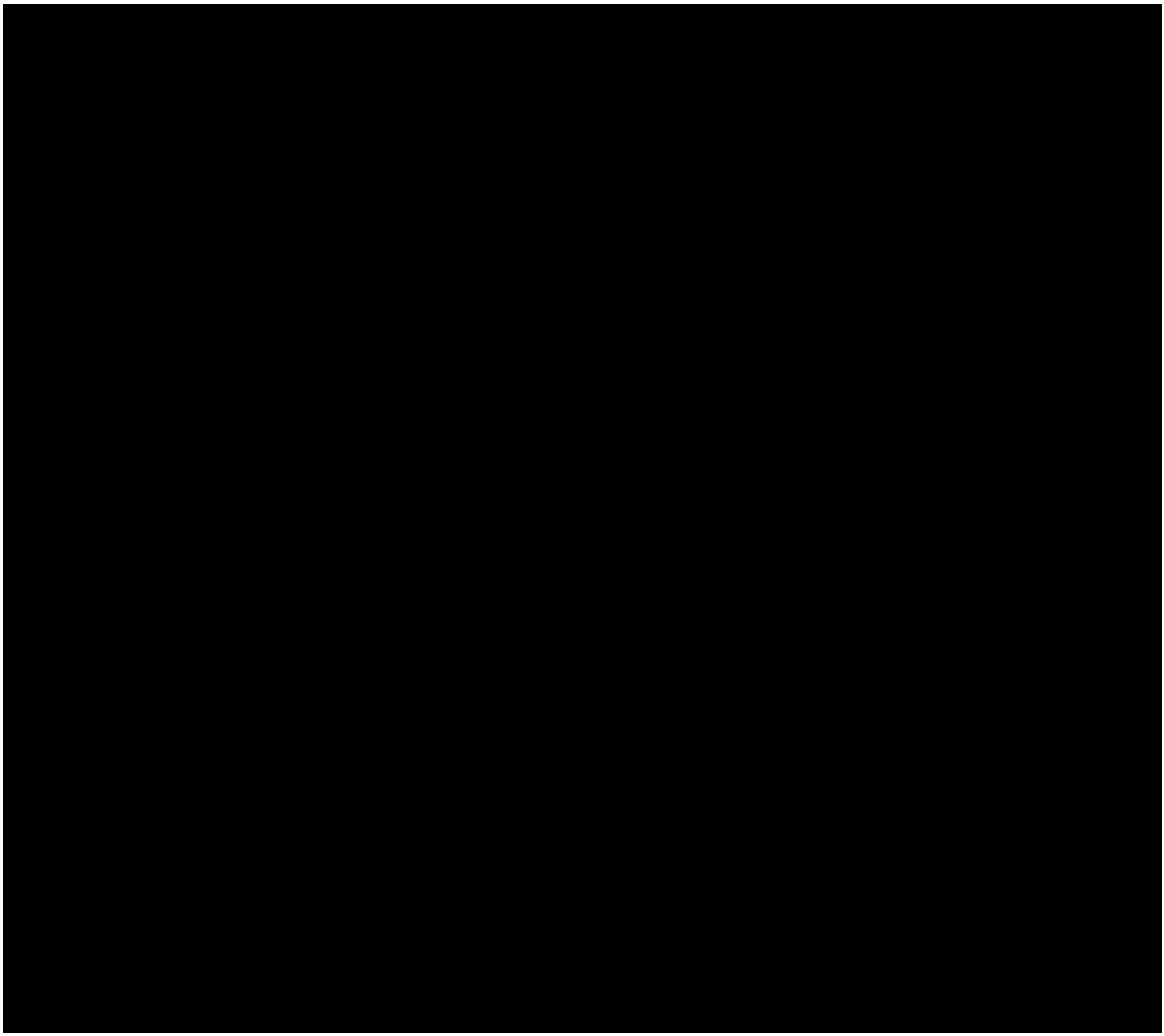

This structural low allowed Pacific Ocean water to enter the basin—a connection that was fully established by the Middle to Late Callovian. Deposition within the basin switched from primarily terrestrial facies to a hypersaline, restricted-marine facies (Galloway, 2008). This switch is recorded by the widespread deposition of evaporitic deposits, collectively referred to as the Louann Salt. The abrupt transition from older, synrift continental deposits to more widespread, marine-influenced evaporitic deposits is commonly used to define the base of the Gulf of Mexico basin fill succession (Sawyer, 1991; Galloway, 2008).

Accelerated extension caused by Callovian-age crustal rupture, emplacement of basaltic crust, and increased seafloor spreading rates resulted in the termination of widespread evaporitic deposition in the basin. By the end of the Early Cretaceous, spreading centers had shifted east into the Atlantic and Caribbean basins. As a result, the crust underpinning the Gulf of Mexico basin began to cool and subside.

A series of basin-rimming Aptian-Albian carbonate platforms (i.e., Sligo Formation, James Limestone, Rodessa Formation, and Glen Rose Limestone, to name a few) developed on the more slowly subsiding basin margin (Winker and Buffler, 1988). Clastic sediments were largely constrained to an area inboard of the platform carbonates along the periphery of the basin. It was at that time that the Gulf of Mexico achieved its current morphologic form. These carbonate platforms ultimately drowned in the Late Cretaceous due to high, load-driven subsidence rates. By the start of the Cenozoic, clastic depositional systems previously constrained to the basin margin begin to prograde and fill the basin—and this process continues through today (Figure 1-2).

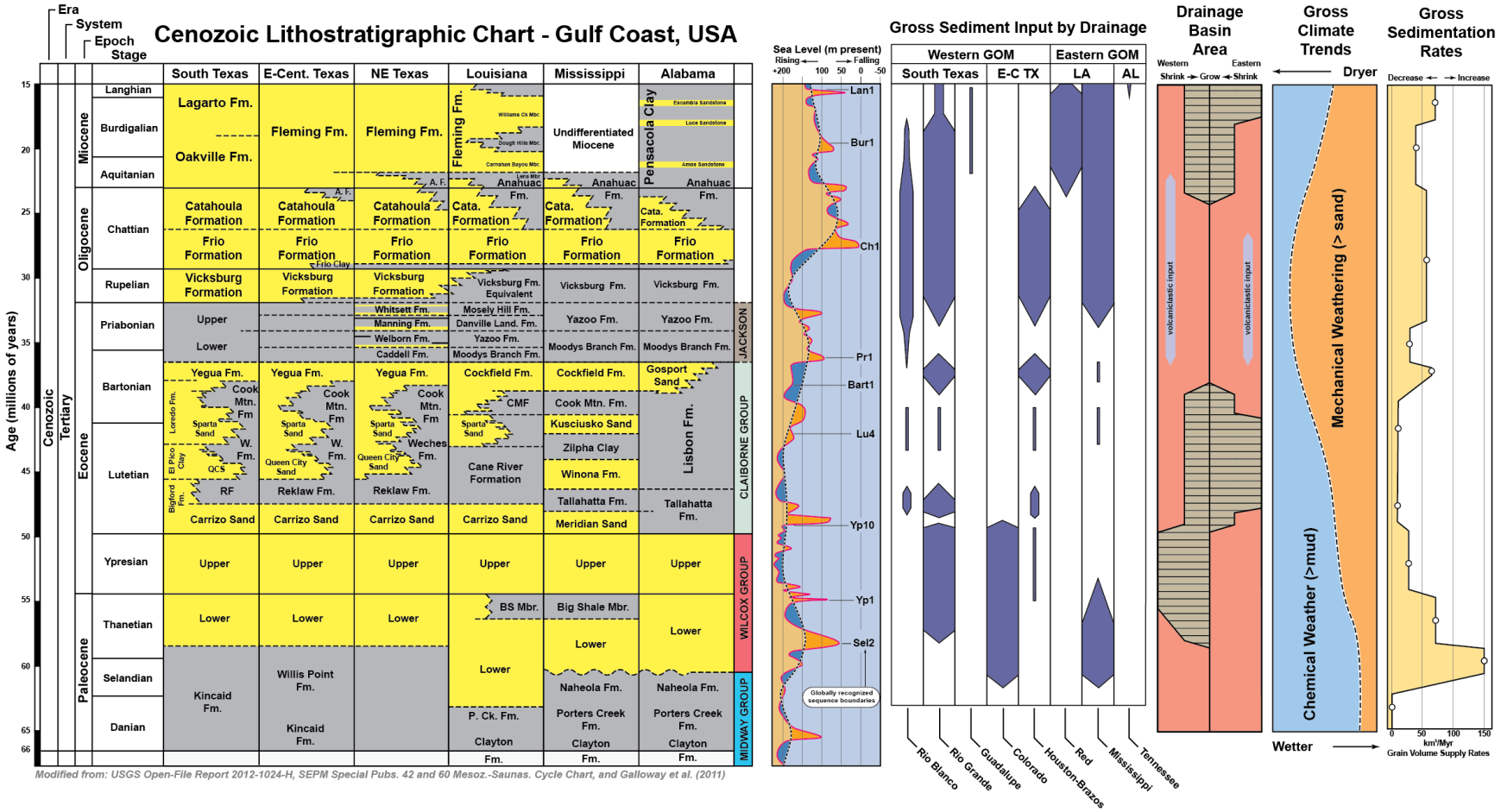

Figure 1-2 – Lithostratigraphic correlation chart for the northern portion of the Gulf of Mexico basin (left). Yellow formations represent more sandy intervals, and gray formations represent more muddy intervals. A comparison of stratigraphic forcing mechanisms, relative to the development of formations within the basin, are shown to the right.

Paleoclimates, Eustasy, and Fluvial Drainage Area Evolution – Greater Gulf of Mexico Region

The Cenozoic fill succession records the climatically modulated delivery of sediment from the interior of the continental United States to the Gulf of Mexico basin. Although long-term climatic trends played an important role in the style, scale, and sediment flux of fluvial delivery systems to the Gulf of Mexico basin, far-field tectonic influences and modification of the paleo-landscape played an equally important role in the development and evolution of catchment areas and drainage-basin networks (Figure 1-3). As sediment was delivered to the basin margin, eustasy and relative sea level had a profound influence on the location and style of deposition, depositional body morphology, and stratal stacking patterns within the coastal to fully marine portions of the receiving basin.

Galloway et al. (2011) provided a detailed description of Cenozoic forcing mechanisms, their variability through time across the continental interior and Gulf Coast regions of the United States, and maps of drainage basin evolution. Figure 1-3 summarizes observations from Galloway et al. (2011) concerning sediment supply to the major Gulf of Mexico depocenters through the Cenozoic. This figure also illustrates the timing and location of key sequence stratigraphic surfaces, long-term stratal stacking trends, and the development of reservoir-seal couplets in the basin.

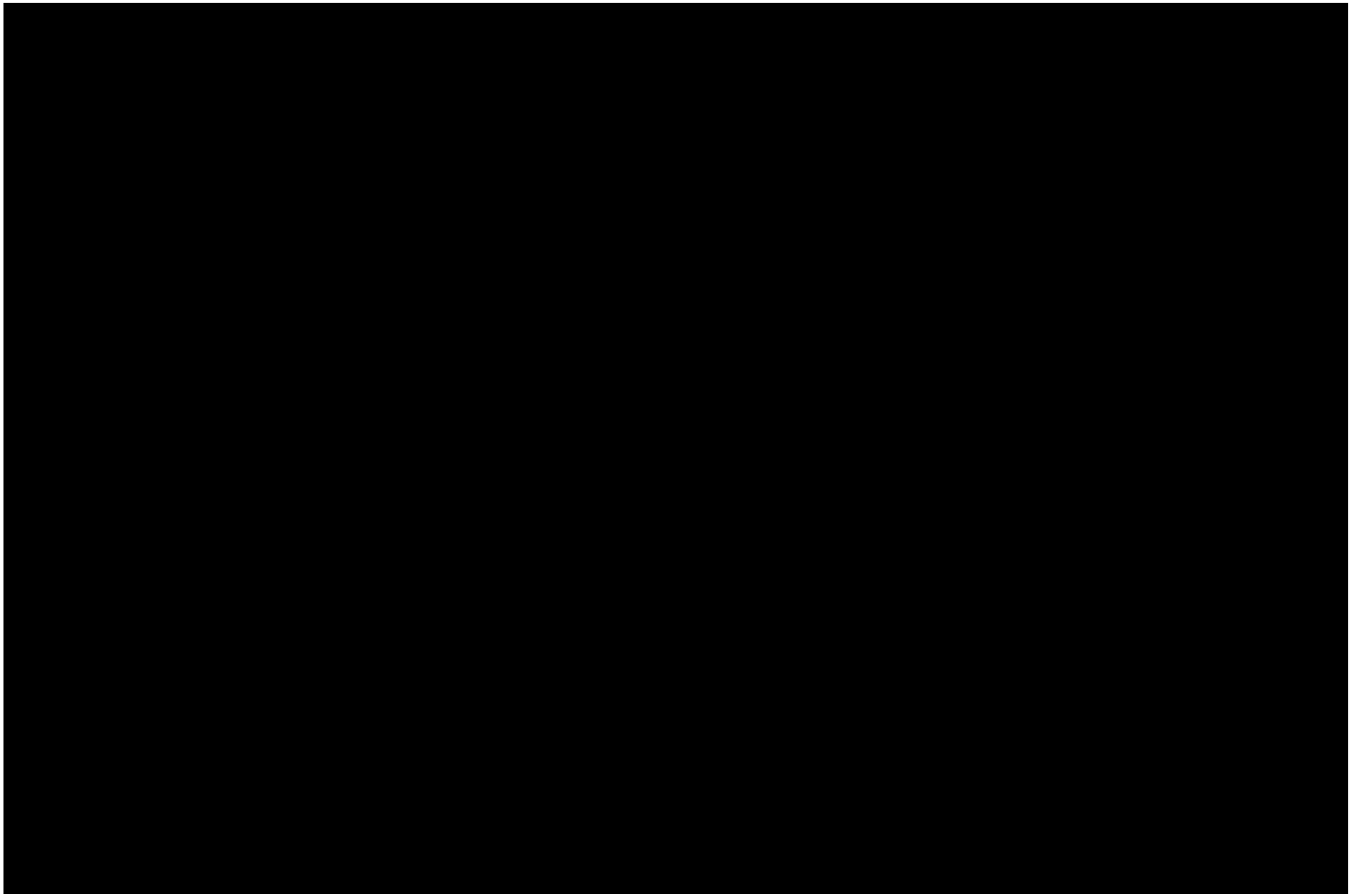

Northern Gulf of Mexico Basin Cenozoic Fill Succession

The Cenozoic fill succession is characterized by a largely progradational stack of both ramp-style and passive margin-style continental shelves (Figures 1-4 through 1-6). The overall pattern of south-directed progradation reflects, in part, the load-driven generation of accommodation due to the overall deepening of the Gulf of Mexico basin. Loading also played a major role in the deformation of the northern Gulf of Mexico. Observed deformation can be separated into three different but interrelated styles: (1) extensional faulting and failure of the distal portions of coastal prisms and/or continental shelf edges along large, down-to-the-south, mostly listric faults; (2) Louann Salt migration associated with differential loading and development of salt diapirs, stocks, canopies, welds, and salt evacuation mini-basins; and (3) far-field tectonic effects associated with Laramide thrusting events in the western interior of the continental United States.

[redacted]

Figure 1-2 summarized many of the key forcing mechanisms that influenced the deposition of major reservoir and seal systems across much of the basin. With respect to this permit application, the focus will be on the [redacted]—the injection interval and confining system in the Mockingbird Project. [redacted]

Figure 1-7 illustrates the distribution of the [redacted] strata within the preferential window or zone for potential CS projects. The observed reservoir types, qualities, thicknesses, and connectivity change across the zone are strongly influenced by proximity to drainage basin outlets (depocenter); hinterland mineralogy and timing of sediment delivery to the coast; coastal marine processes at and between primary depocenters; local tectonics; and the position and direction of the sea-level fluctuations through the [redacted]. The genetically [redacted] form a southward prograding coastal prism consisting of fully marine, marine-influenced fluvial, fluvial, and coastal plain deposits. The form of this coastal prism was modified by extensional faulting and salt-related folding and by younger faulting, but reconstructions indicate that the [redacted] system had a typical, passive margin-type shape—and that the youngest shelf-slope break parallels the modern-day shoreline along the Texas sector of the Gulf Coast (Figure 1-3).

The primary [redacted] in western Louisiana consist primarily of the clean, shallow marine deltaic and correlative wave-dominated shoreface deposits of the [redacted]. Major depocenters at the mouth of the Houston-Brazos system in eastern Texas and the Mississippi system in central Louisiana were receiving significant volumes of sediment at this time (Galloway et al., 2011). In the Mockingbird Project area, a large, river-dominated deltaic complex (referred to herein as the Mississippi delta) with attached wave-dominated strandplains formed (Figure 1-3).

Observed increase in sediment supply during the Early Oligocene is partially in response to crustal uplift in the southwestern-to-western source areas of the drainages the Gulf of Mexico (Galloway et al., 2011), where Cretaceous through Early Cenozoic foreland basin fill in the western interior of the United States was uplifted some 3 kilometers (Gray et al., 2001). As a result, surface gradients during the Oligocene were relatively steep in the hinterland, and fluvial systems likely became more efficient at delivering sediment to the Gulf of Mexico basin. Arid climatic conditions dominated during Oligocene time. Therefore, mechanical weathering outpaced chemical weathering in the hinterland, generating an overabundance of reservoir-grade sands that could be delivered to the Mississippi delta.

Records of global sea-level fluctuations (Figure 1-2) indicate that the position of sea level was significantly higher in the Eocene than during the ensuing Oligocene. This overall trend from relatively high to substantially lower sea-level positions in the Gulf of Mexico is reflected in the stratal stacking patterns and lithologic assemblages in the basin, indicating that eustatic effects played a major role in the spatial and temporal position of shorelines and key reservoirs, and the development of internal and ultimate sealing intervals within the Oligocene and into the Early Miocene. Figure 1-2 illustrated the observed stratal architecture for the Paleocene through Early Miocene sediments in the eastern Texas and western Louisiana sectors of the Gulf of Mexico basin, as well as the interplay of forcing mechanisms on the development of Oligocene-Miocene reservoir-seal units.

The Cenozoic fill succession has a predictable stratigraphic stacking pattern that reflects the influence of sea-level fluctuations, basin subsidence associated with hydrodynamic- and sediment-driven loading—down to the basin extensional faulting associated with the failure of paleoshelf margins—and variations in sediment flux associated with the long-term growth or demise of coastal drainage systems. Overall, the stratal architecture of the Cenozoic can be characterized as a series of progradational, sand-prone wedges separated by a series of more muddy, transgressive marine intervals, each of which has a moderately well-developed maximum flooding surface (MFS), an interval of slow deposition that often has exceptional sealing characteristics (Figure 1-6). Although this stratal architecture has a predictable stacking pattern, the interpretation of the Cenozoic is in places problematic due to structural modification related to high subsidence rates away from the basin margin, which result in the southward bending and deepening of the Cenozoic and older stratigraphy south of a major hinge line. Furthermore, much of the northern portions of the various formations have been removed by Late Cenozoic erosion centered on this hinge line area.

The Cenozoic fill is interpreted as a series of southward-directed, downward-stepping clastic wedges that form a highstand sequence set. Overall, lowstand deposits appear to be a secondary reservoir type in the basin, most likely due to high subsidence rates that reduced the depth and extent of fluvial erosion associated with the fall of sea level and extension of fluvial systems onto and across the exposed inner paleoshelf. The reservoir succession in the F-C interval is interpreted as a series of thick, downstepping or offlapping, sandy highstand and falling-stage systems tracts, with a minor component of muddier lowstand systems tracts that are mostly south of this study area. The F-C interval is underlain by a major transgressive interval (referred

to herein as the Claiborne interval and the Vicksburg). [redacted]

Furthermore, the sea-level falls through the Miocene increased in frequency and extent, as did the sediment yield to the basin. This resulted in the next major regressive phase of deposition and development of the [redacted]. During deposition of the formation, accommodation along the basin margin was somewhat limited. This resulted in a series of rapidly basinward-stepping shorelines and highly progradational and slightly downstepping shelf margins. In the Mockingbird Project area, the marine portion of the Fleming Formation is constrained to the bottom, oldest reservoir intervals. For the most part, the Fleming consists of sandy fluvial channel belts and more muddy floodplain complexes in the project area.

Figure 1-7 depicted the detailed stratigraphic interpretation of the [redacted] in the Mockingbird Project area. The attempt here was to define key lithostratigraphic surfaces and interpret staking patterns and depositional facies across the area. Based on the well-log character and seismic interpretations, [redacted]

[redacted]

1.3 Site Geology

The AOR, located in Allen Parish, Louisiana (Figure 1-8), is defined by the combination of the maximum critical pressure front and stabilized CO_2 plume for all intervals (*Section 2 – Plume Model*). Geological properties and characterization of the injection and confining zones within the AOR are drawn from proprietary, licensed, subscribed, and public data sources. The existing data within the AOR consists of [redacted]

Data from existing wells in Allen Parish, published literature, and publicly available data sets including the Louisiana Department of Energy and Natural Resources (LDENR) and the Louisiana Geological Survey (LGS), IHS LogNet, Enverus, and Core Laboratories' Reservoirs Applied Petrophysical Integrated Data (RAPID) service were used to characterize the subsurface. General geologic setting and lithological attributes are described regionally from publications and offset well log data in the project area. For regional characterization, 2D and 3D seismic data were used as the main source for structure framework horizon mapping, and [redacted] legacy wells were chosen to perform well top correlations to adjust/fine tune the seismic interpreted horizons in depth. For geomodel facies distribution, [redacted] wells were used for the modeling; the available logs for those wells are listed in *Appendix B-2*. A seismic cross section through the proposed Mockingbird Injection Wells (INJ) No. 01, No. 02, No. 03, and No. 04 is shown in Figure 1-9. Key stratigraphic layers are described in this section, while faults and fault seal properties are described in *Section 1.5*.

ExxonMobil has applied for a Class V permit to drill a stratigraphic test well, Mockingbird In-Zone Monitoring Well (IZM) No. 01. A draft permit has been issued and is currently out for public notice. If the permit is issued, ExxonMobil plans to drill Mockingbird IZM No. 1 [redacted] with the purpose of gathering subsurface geological data to support pre-injection data requirements for the proposed project.

Four offset wellbores with log coverage are proximal to the proposed injection wells as follows:

- [redacted]

All of the above wells extend from above the upper confining zone (UCZ) to below the top of the lower confining zone (LCZ). Depths and associated thicknesses of the UCZ, secondary intraformational seals, injection intervals, and LCZ encountered in these wells are listed in Table 1-1. Figures 1-10 and 1-11 show well cross sections (north-south, east-west, respectively) with Vshale, resistivity (where available), formations, and depths for multiple wells within and proximal to the AOR.

[redacted], showcases key stratigraphic surfaces and interpreted depositional facies across the study area. Based on the well-log character and regional interpretations, [redacted]

[redacted]

[redacted]

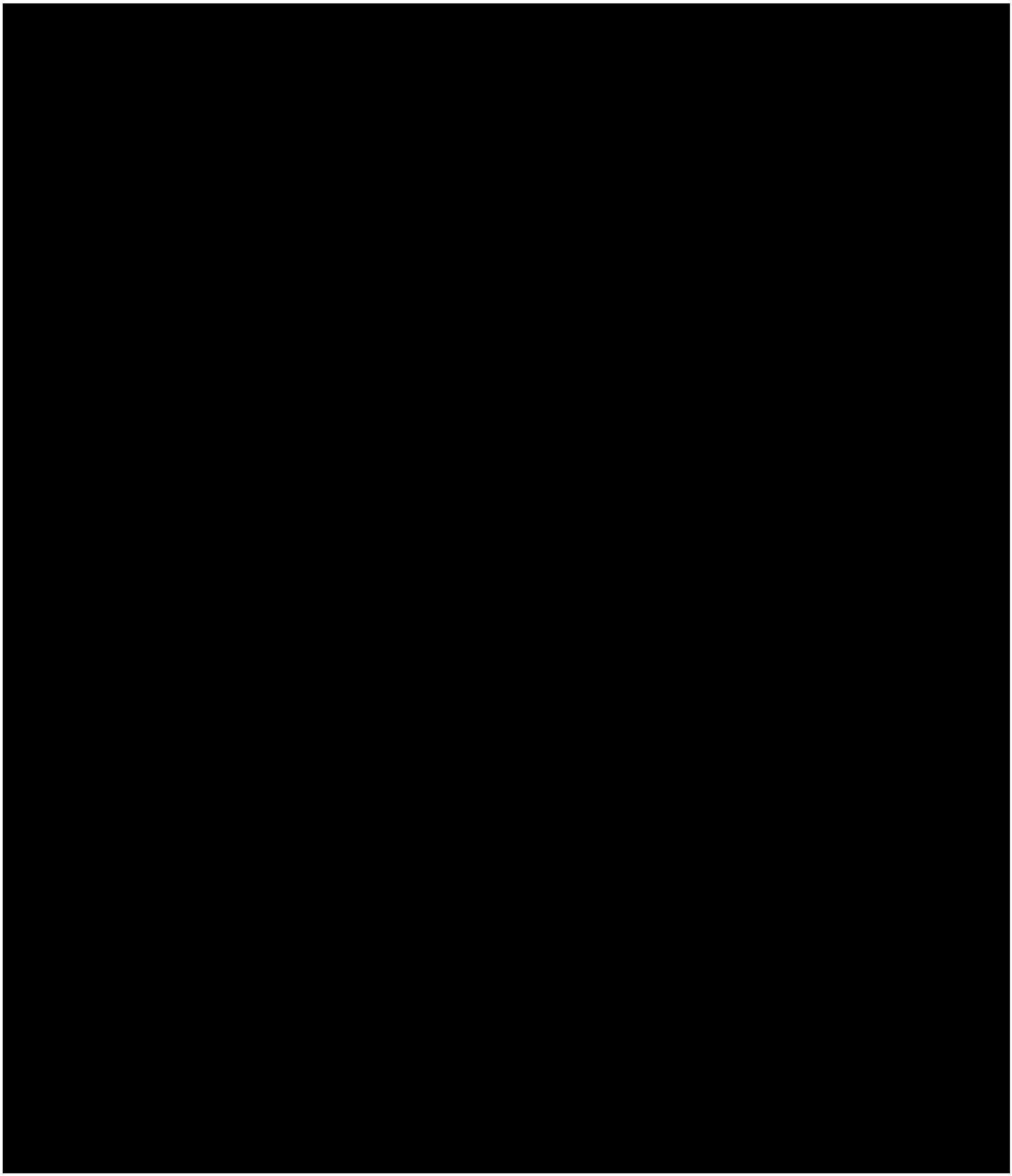

1.3.1 Injection Zone

The injection zone is composed of the [redacted]. The different injection intervals are separated by a mix of regionally extensive shales, and more locally extensive intraformational shale. Depth structure maps and thickness maps for the injection intervals are shown in Figures 1-13 and 1-14, respectively. Reservoir properties for the sands within the injection zone average from [redacted] for porosity and [redacted] millidarcy (mD) for permeability (discussed in *Sections 2.5.6* and *2.5.7*). Because of the well density and compressed scale of the maps in these figures, *Appendix B-2* provides a table (Table B2-1) with pertinent well information and a detailed map (Figure B2-1) showing well locations relative to the AOR.

The [redacted] targeted for injection are composed of interbedded sandstones, siltstones, and shales sourced primarily from the paleo-Mississippi River system and [redacted] The Early [redacted] within the project area contain primarily prograding to downstepping, [redacted]. By the Late [redacted] the environment of deposition (EOD) had transitioned [redacted] The Early [redacted] g EOD is primarily an [redacted]

[redacted]

Figures 1-10 and 1-11 showed Vshale logs derived from spontaneous potential (SP) logs that capture the stratigraphic variability of interbedded sands, siltstones, and shales in the [redacted]. This injection interval sits immediately below the Catahoula at 4,500–[redacted] within and proximal to the AOR (Figure 1-13a). The [redacted] injection interval is separated from the UCZ (*Section 1.3.2.2*) by the [redacted] (intervals that are not targeted for injection in this permit application). Within the AOR, the average gross thickness of the [redacted] (Figure 1-14a).

[redacted]

Figures 1-10 and 1-11 showed the stratigraphic variability of interbedded sands, siltstones, and shales in the [redacted]. The [redacted] is separated from the [redacted] above by an interval of locally extensive shales that can be correlated across the AOR. Stratigraphic variability in the [redacted] is similar to that observed in the [redacted]. Within the AOR, the [redacted] (Figure 1-13b), and the average gross thickness of the [redacted] (Figure 1-14b).

[redacted]

Figures 1-10 and 1-11 also showed the stratigraphic variability of interbedded sands, siltstones, and shales in the [redacted]. The [redacted] is separated from the

[redacted] above by an interval of regionally extensive shales. Stratigraphic variability in the [redacted] is similar to that observed in the [redacted] Within the AOR, the [redacted] (Figure 1-13c), and the average gross thickness of the [redacted] (Figure 1-14c).

1.3.2 Confining System

The confining system for the Mockingbird Project protects the USDW and is comprised of a primary UCZ, the intraformational [redacted] seal, and the LCZ (Figures 1-10 and Figure 1-11). Containment intervals include the UCZ, the intraformational [redacted] seal, and thinner intraformational shales throughout the [redacted] which provide additional baffling and sealing capacity above and between injection intervals. Thicknesses and seal properties are derived from offset well data; these will be complemented by pressure, temperature, geomechanical, and mineralogical data collection planned in the stratigraphic test well (Mockingbird IZM No. 01). Depth structure maps and thickness maps for the confining intervals are shown in Figures 1-15 and 1-16, respectively. Reservoir properties for the confining system are estimated from legacy data at [redacted] porosity and less than [redacted] for permeability (*Sections 2.5.6* and *2.5.7*). *Appendix B-2* provides a table (Table B2-1) with pertinent well information and a detailed map (Figure B2-1) showing well locations relative to the AOR for all wells used to generate the thickness maps.

[redacted]
The UCZ lies immediately above the [redacted]. Figures 1-10 and 1-11 showed the UCZ, which can be correlated across the AOR with the top depth ranging from [redacted] feet TVDSS (Figure 1-15a). The average gross thickness of the UCZ is [redacted] above the proposed injection zone within the AOR (Figure 1-16a). The UCZ is [redacted] that was deposited during a regional transgression and is a regionally extensive stratigraphic package correlated across Allen Parish. [redacted] (*Section 1.5.2*).

[redacted]
The next major sealing interval is the [redacted] which was deposited during a regional flooding event between deposition of the [redacted] and [redacted] formations. Within the AOR, the [redacted] is at [redacted] (Figure 1-15b) and has a gross thickness of [redacted] (Figure 1-16b).

Multiple shales [redacted], that are below the UCZ, above the Anahuac intraformational seal, and within the [redacted] formations (sandy intervals that are not injection targets), provide further baffling and withholding to vertical flow.

The [redacted] are separated by locally extensive, thinner [redacted] intraformational shales that can be correlated across the AOR and that add redundant sealing capacity for the [redacted] (Figures 1-10 and 1-11).

[redacted]
The LCZ is roughly [redacted] thick within the AOR (Figure 1-16c), extending from the top of the [redacted] TVDSS (Figure 1-15c). The LCZ extends through the [redacted] to the base of the [redacted], and—for the purpose of this study—the [redacted] is not subdivided from the [redacted] interval (Figures 1-10 and 1-11).

Within the vicinity of the AOR, the [redacted] is composed of carbonaceous mudstone, and the [redacted] primary lithology is also mudstone with local thin sands and silts (Figure 1-7).

1.4 Porosity

1.4.1 Well Data

Petrophysical evaluations were performed on [redacted] to estimate shale volume (VSH) and total porosity (PHIT) from wireline logs. For the [redacted] wells evaluated, all wells had either an SP or gamma ray (GR) log to estimate shale volume. Of those wells, [redacted] had either a compressional sonic (DTC) and/or bulk density (RHOB) log to estimate total porosity across the formations of interest. Table B2-2 in *Appendix B-2* lists the wells and log data, including neutron porosity (NPHI), available for analysis.

1.4.2 Log Quality Control

Many legacy wells were affected by poor borehole conditions, therefore additional steps were required to ensure consistent petrophysical properties between the wells. These steps are discussed in greater detail in the following section.

1.4.3 Methodology

1.4.3.1 Shale Volume

Shale volume was primarily determined from the SP log. The SP logs were baselined in thick shales to read zero millivolts (mV), and clean sand values were interpreted for each well based on the magnitude of the SP deflection. Shale volume was then calculated from the SP log as follows in Equation 1:

(Eq. 1)

$$VSH\_SP = \left\lfloor \frac{SP_{log} - SP_{clean}}{SP_{shale} - SP_{clean}} \right\rfloor$$

In the absence of an available SP log, the GR log was used to calculate shale volume. Similar to the SP approach, the GR logs were bulk-shifted to read approximately 100 GAPI in shales, and clean sand values were interpreted for each well. Shale volume was then calculated from the GR log as follows in Equation 2:

(Eq. 2)

$$VSH\_GR = \left\lfloor \frac{GR_{log} - GR_{clean}}{GR_{shale} - GR_{clean}} \right\rfloor$$

1.4.3.2 Total Porosity

Compressional sonic was the most common porosity log available. To compute total porosity, the method proposed by Raymer et al. (1980) was used. This method is particularly well-suited for high-porosity, unconsolidated sands typical of the Gulf Coast region. Additionally, a "Shale Reduced" option was selected to correct the high apparent porosities related to increasing shale

content (i.e., due to an increase in measured slowness). Total porosity from the sonic logs was calculated as follows in Equation 3:

(Eq. 3)

$$DT_{SR} = \text{maximum}\left[DT_{ma}, \left(\frac{DT_{log} - V_{sh} * DT_{sh}}{1 - V_{sh}}\right)\right]$$

$$\emptyset_S = \left[C * \left(\frac{DT_{SR} - DT_{ma}}{DT_{SR}}\right) * (1 - V_{sh})\right] + (V_{sh} * \emptyset_{sh})$$

where DT_{SR} is the shale-reduced slowness, DT_{sh} is the measured shale slowness from sonic logs, Φ_S is the sonic-derived total porosity, and Φ_{sh} is shale porosity (assumed or known a priori). Table 1-2 provides the parameters used for calculating sonic-derived porosity.

Table 1-2 – Parameters for Calculating Sonic-Derived Porosity

Parameter	Value or Function
Compaction Factor, *C*	[redacted]
Matrix Slowness, DT_{ma}	55.5 µs/ft (default for sandstones)
Shale Slowness, DT_{sh}	10 ^ (2.205 - 0.0000285 * DEPTH + 0.000000001 * DEPTH^2)
Shale Porosity, $\emptyset_{sh}$	0.15

*µs/ft – microseconds per foot

Bulk density logs were used to estimate total porosity in six additional wells. In general, estimating porosity from bulk density logs is more straightforward, since any increase in shale content typically results in a higher measured bulk density (or lower apparent porosity). However, as noted previously, many legacy wells were affected by borehole washouts, which adversely impacts the bulk density measurement. Consequently, a similar approach using shale volume was implemented where density-derived porosity was calculated as follows in Equation 4:

(Eq. 4)

$$\emptyset_D = (1 - V_{sh}) * \left(\frac{\rho_{ma} - \rho_{log}}{\rho_{ma} - \rho_f}\right) + V_{sh} * \theta_{sh}$$

where Φ_D is the density-derived total porosity, ρ_{ma} is the matrix density, and ρ_f is the fluid density. Table 1-3 provides the parameters used for calculating density-derived porosity. A total porosity ($\emptyset_T$) equation follows in Equation 5.

Table 1-3 – Parameters for Calculating Density-Derived Porosity

Parameter	Value
Matrix Density, ρ_{ma}	2.65 g/cm^3 (default for sandstones)
Fluid Density, ρ_f	1 g/cm^3
Shale Porosity, ϕ_{sh}	0.15

*g/cm^3 – grams per cubic centimeter

(Eq. 5)

$$\emptyset_T = \frac{(\emptyset_D + \emptyset_{RES})}{2} \; or \; \emptyset_T = \frac{(\emptyset_S + \emptyset_{RES})}{2}$$

where ϕ_{RES} is the conductivity-derived porosity.

(Fleming) $$\emptyset_{RES} = -0.425 + 0.21 * LOG10(COND)$$

(Frio/Catahoula)

$$\emptyset_{RES} = -1.77 + 0.905 * LOG10(COND) - 0.091 * LOG10(COND)^2$$

1.5 Geologic Structure

Regional dips are gentle and vary on average between [redacted] within the AOR (Figure 1-17). Higher dips around faults are either artificial (due to gridding artifacts) or due to near-fault deformation.

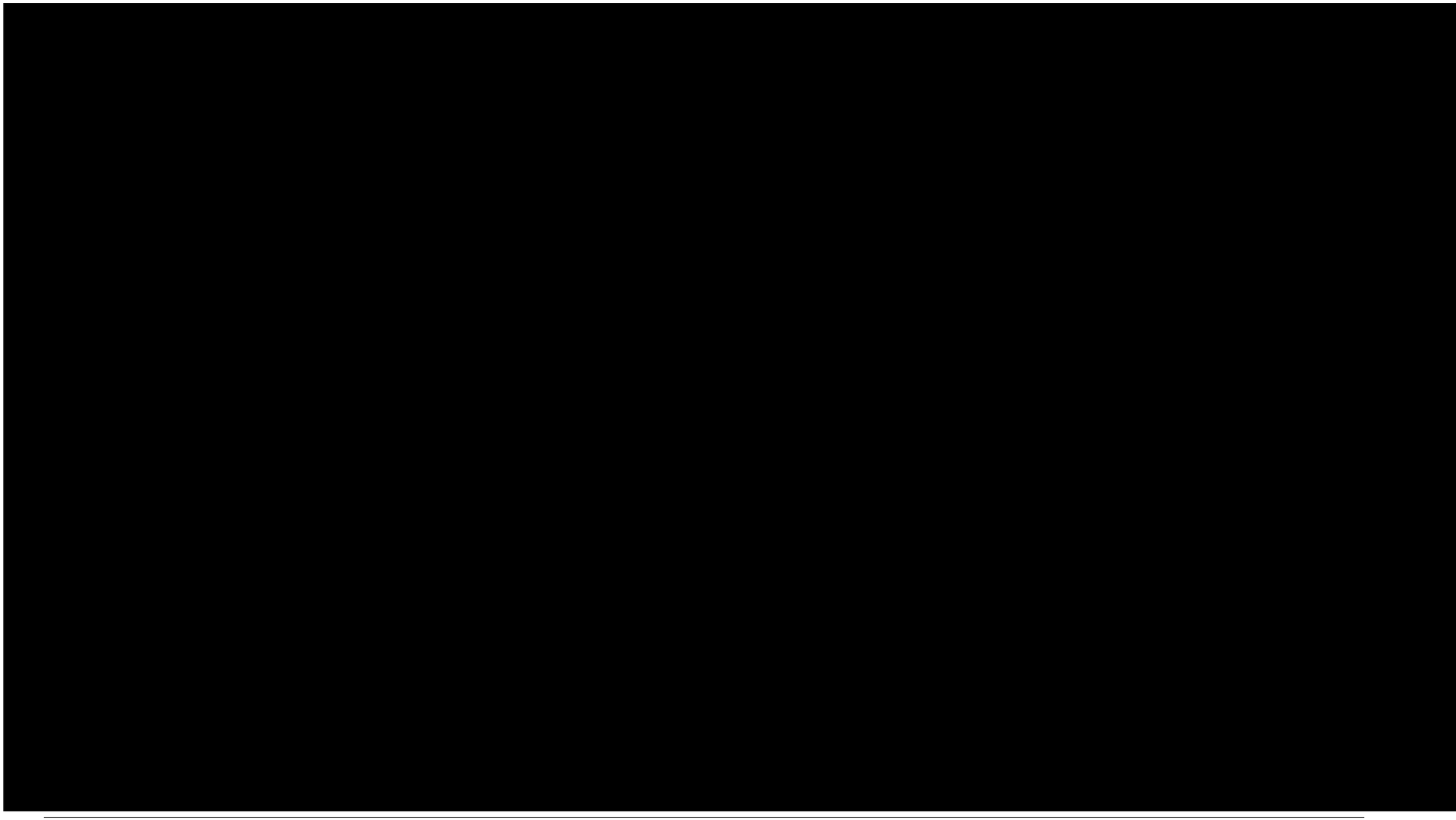

1.5.1 Seismic Survey Data

In creating the geomodel for the Mockingbird Project, 3D seismic data were used that cover [redacted] (Figure 1-18)—in particular, the merged [redacted] (Seismic Exchange Inc.) and the [redacted] (Seitel). The [redacted] volume in the project area is comprised of the [redacted], and the [redacted] was stand-alone. The bin size was 110 x 110 feet, with a maximum offset of 38,310 feet for the [redacted] and 20,000 feet for the [redacted] The common mid-point (CMP) fold was approximately 74 for the [redacted] and 50 for the [redacted].

[redacted]

The wells that contained enough data to perform a well tie (i.e., tie the seismic survey to depth and allow the correlation of historical well logs to seismic data) in proximity to the Mockingbird Project were the J [redacted] The map in Figure 1-18 shows the location of these wells relative to the project AOR. A zero-phase Ricker wavelet with a peak frequency of 25 Hertz (Hz) was used to perform the ties. The results of the well ties are shown in Figures 1-19 through 1-22.

Time-depth relationships were generated from the respective sonic logs, and all four wells offered good ties for the purposes of geologic characterization at the project site. High-quality well ties, as discussed in this section, yield a good conversion of the seismic data from time to depth, allowing for a quality comparison between well data and seismic data. In areas without well control, a regional velocity model was utilized—built from a network of regional 2D seismic data, which yielded sufficient time-depth conversion results as blind-tested at the well locations.

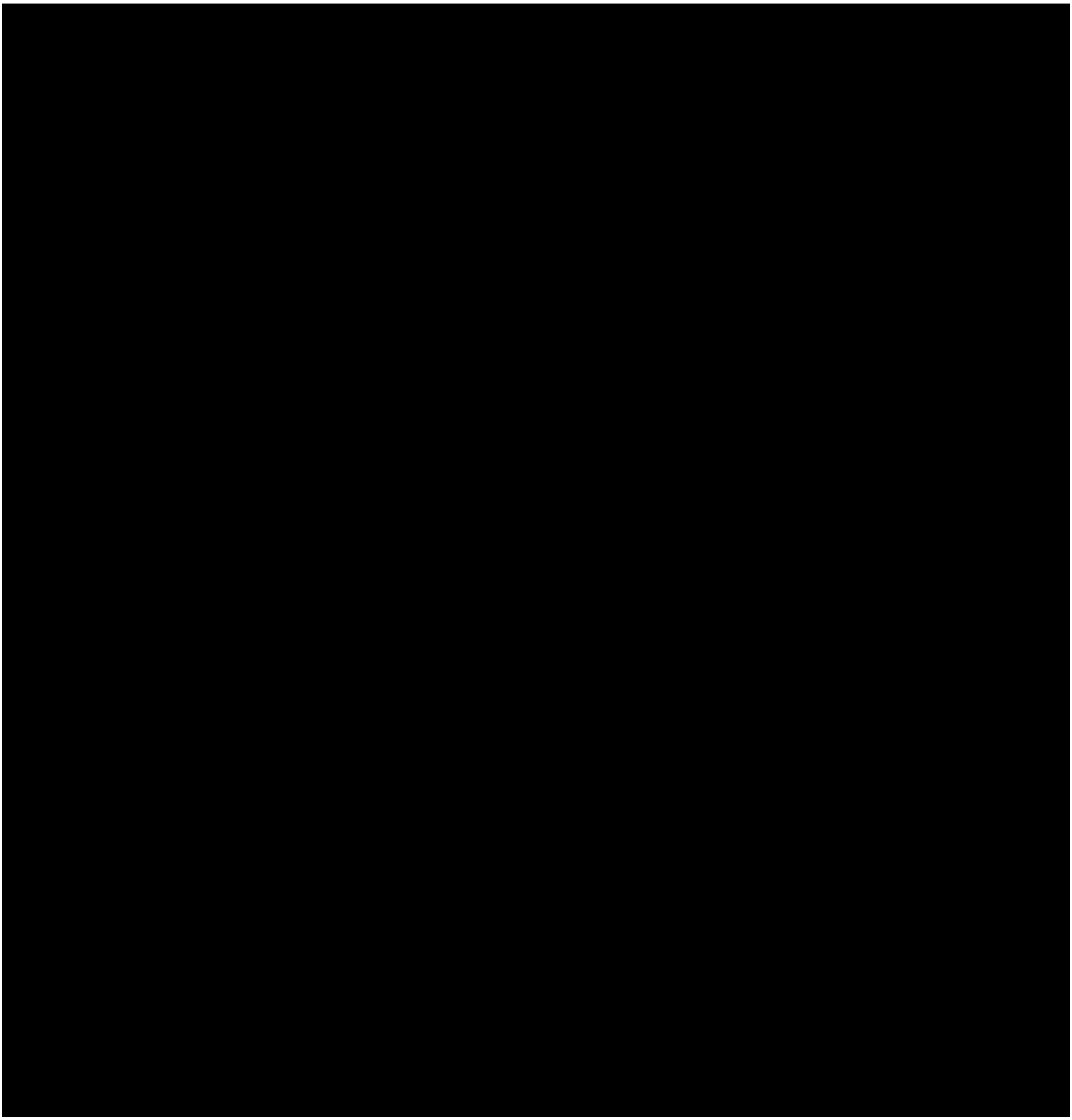

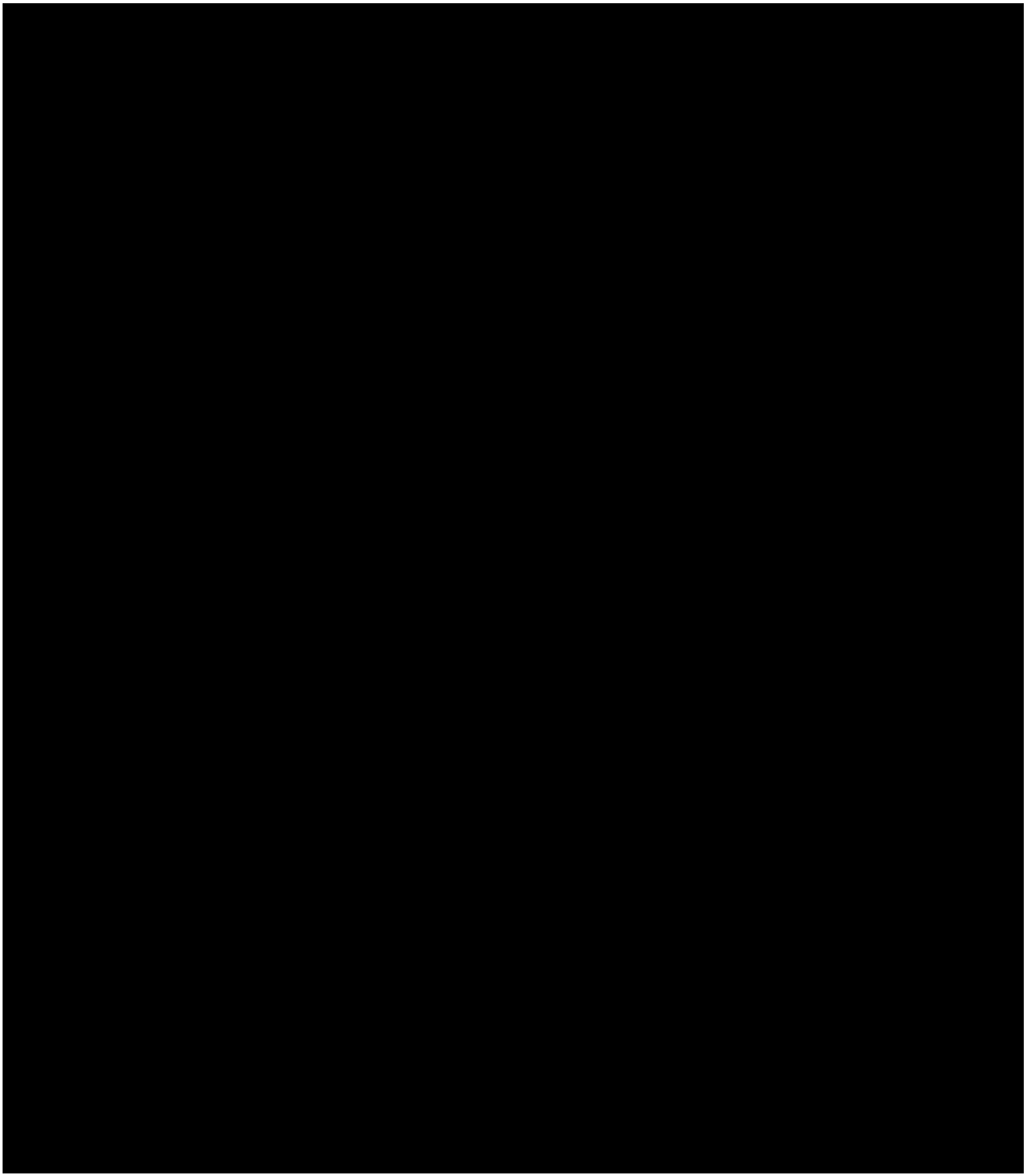

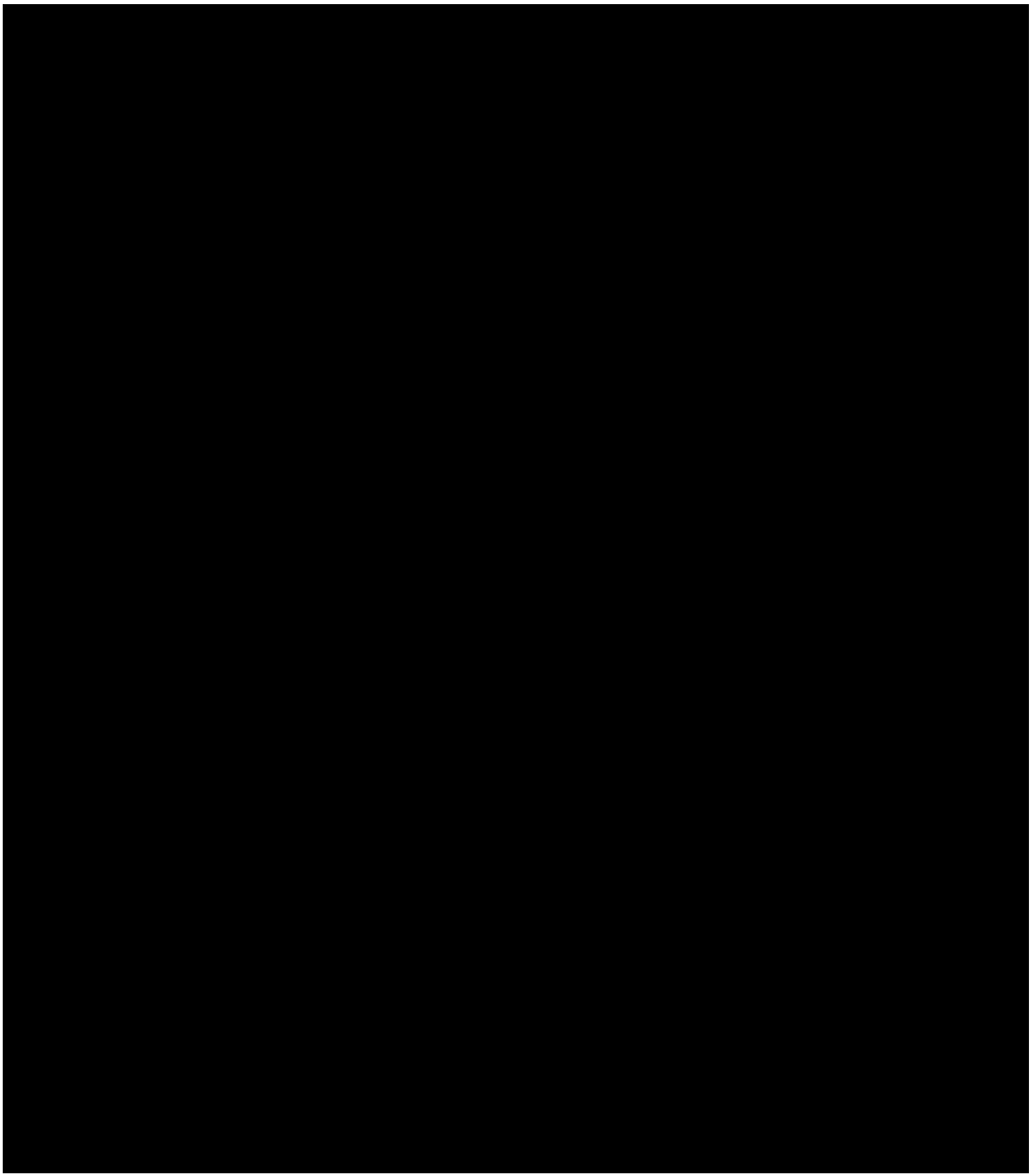

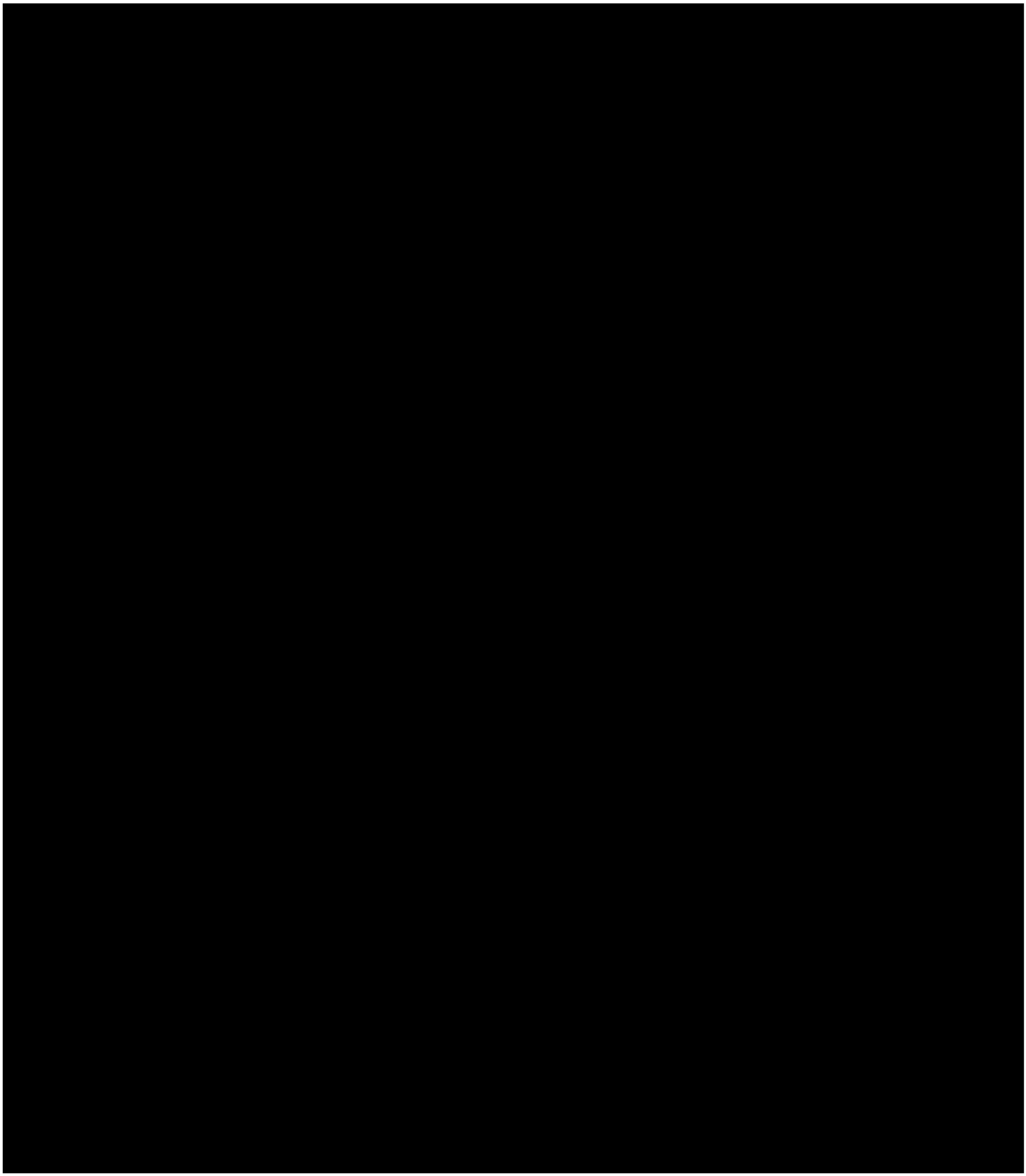

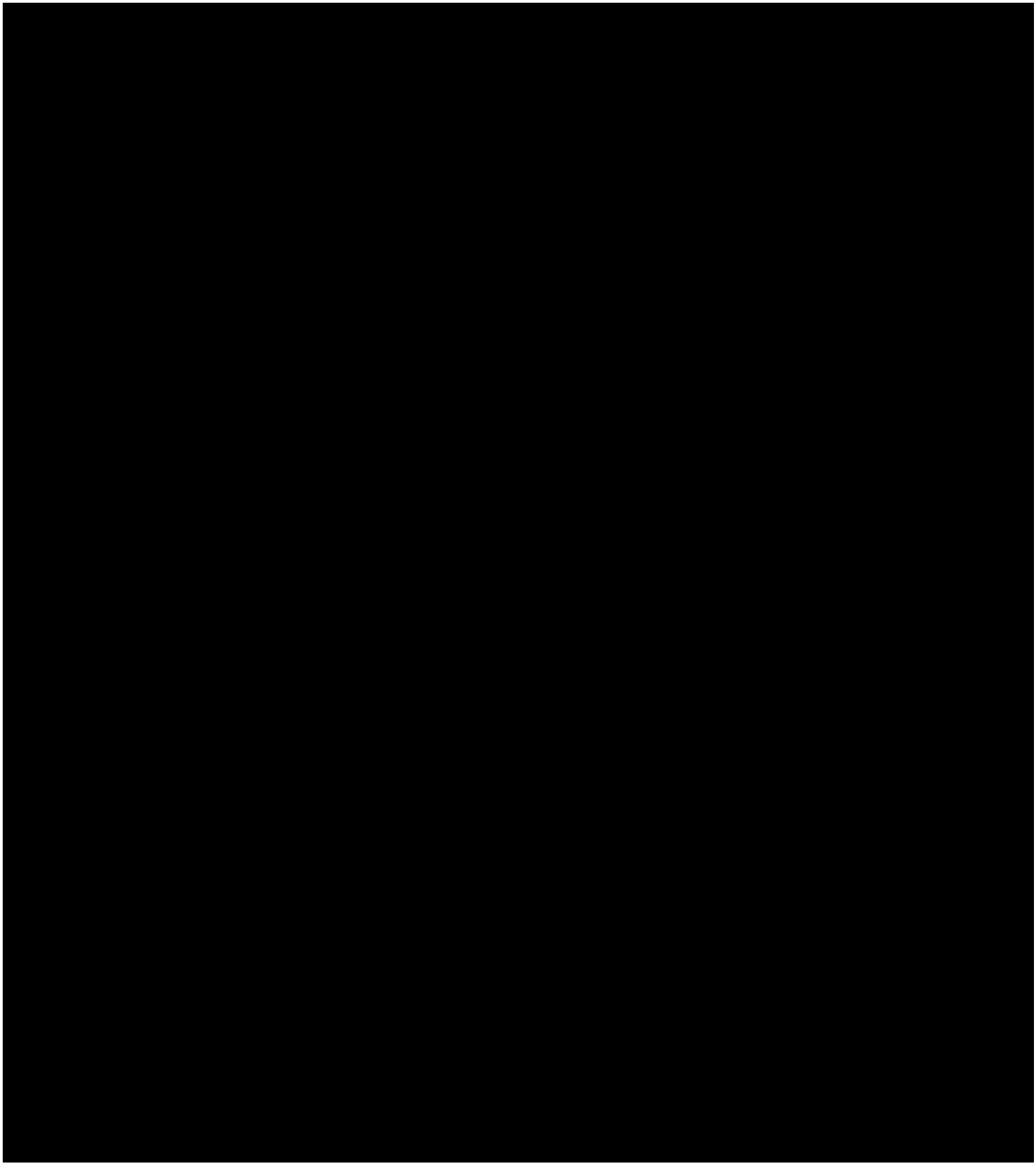

1.5.2 Faults

[redacted] faults were identified within the AOR (Figure 1-23). Subsurface fault geometry was interpreted using 2D and 3D seismic, and surface topographic data was used to map surface escarpments. The faults are part of the [redacted] and are typical of the regional growth fault system that parallels the Gulf Coast in Texas, Louisiana, and Mississippi. Regionally, down-to-the-south displacement is on the order of tens to hundreds of feet in the injection and confining zones, decreasing updip. Most major faults or series of overlapping faults go to the surface, and fault scarps with more than a few feet of surface displacement can be identified using moderate-resolution (10 meters), lidar-derived digital elevation models.

In general, growth in the deeper section combined with greater offset indicates that the major period of movement was prior to deposition of the [redacted]. However, growth in the lower half of the [redacted] indicates some movement during this time, and faults that go to the surface demonstrate more recent displacement—although slip in the Miocene and younger section is generally small, on the order of several tens of feet (Hanor, 1982).

[redacted]. The maximum displacements at the UCZ, the top of the [redacted], and the LCZ are provided in Table 1-5. Fault displacement was measured by manual restoration of offset seismic reflections correlated to, or immediately above or below, key horizon tops. This method for measuring offset was used because stratigraphic heterogeneity and near-fault deformation at this location introduce inaccuracies in modeled fault-horizon intersections. For this reason, modeled fault throw profiles were used as a first-order guide to identify displacement maxima along the sections of the faults within the AOR, where manual restoration was then performed.

The discussion following Table 1-5 summarizes the fault offset and seal analysis within and proximal to the AoR.

The mapped fault trace polygons, proximal and within the AOR, are presented in Figure 1-23 and illustrate where the faults intersect a seismic horizon and relevant formation tops. Detailed seal analyses were conducted for [redacted] faults within the AOR to assess the potential impact to the confining properties of the UCZ and fault transmissibility in the injection intervals. The intersection of faults with the pressure front and/or stabilized CO_2 plume varies depending on the fault. [redacted] (Figure 1-23).

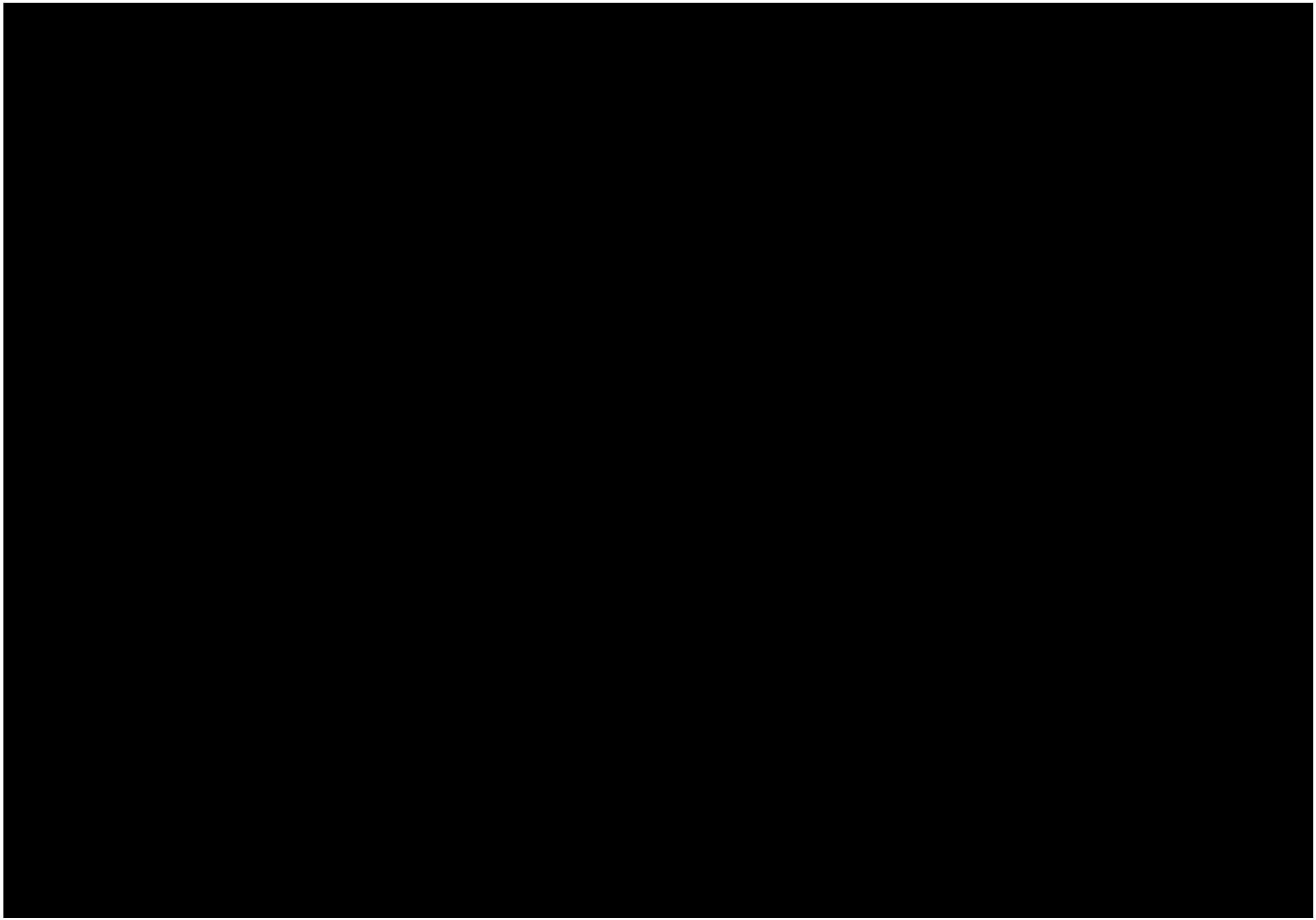

Shale gouge ratio (SGR) calculations to predict the fault seal quality were performed on the faults within the AOR. The SGR methodology is based on Yielding et al. (1997) (Figure 1-24), calculated by Equation 6, which utilizes the zone (lithology), thickness (h), clay fraction (Vshale, estimated from the SP log (*Section 1.4.3.1*)), and the fault displacement (fault throw). Calibrations were based on subsequent methods provided by Manzocchi et al. (1999) and Sperrevik et al. (2002). These calibrations conclude that permeability along the fault is ≤0.01 mD with at least 50% clay fraction, or an SGR more than 0.5, or 50%. For each fault, a well was chosen that (1) penetrates stratigraphy thought to be representative of that containing the most proximal extent of the pressure front and/or CO_2 plume; and (2) was judged representative of other wells along strike of the fault.

The SGR was evaluated using PE Limited's (Petex) MOVE software. On the triangle plots in Figures 1-25 to 1-28, purple strata represent intervals with the highest calculated SGR (greater than 95%), and gray-scale strata represent the SGRs greater than 50%—the conservative threshold above which a fault is sealing (Manzocchi et al. 1999; Sperrevik et al. 2002). The yellow, orange, and red represent areas where the SGR is less than 50%, where faults are more likely to be transmissive. Figures 1-25 to 1-28 show SGR seal-analysis triangle plots for the four faults within the AOR. The SGR analyses were run using the maximum offset at the top of the LCZ. Because displacement decreases updip, this value serves as a conservative overestimate for offset in the [redacted] injection intervals.

(Eq. 6)

$$SGR = \frac{\Sigma(h * VShale)}{Fault\ Throw}$$

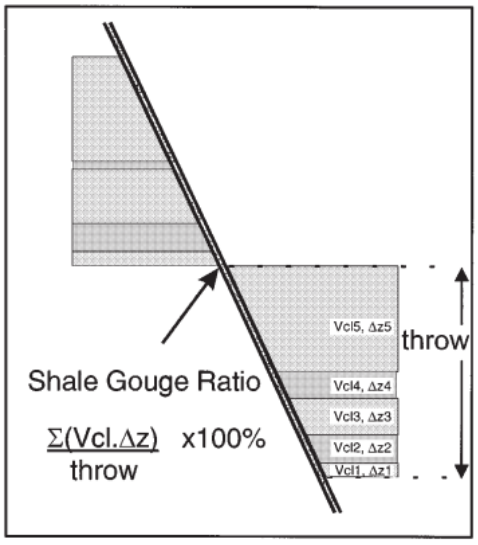

Figure 1-24 – Schematic of SGR Calculation from Yielding et al. (1997)

The local geologic setting is well-suited to the application of the SGR method to assess fault seals, because key geologic data requirements of the SGR method are locally met as follows:

- During fault movement, the stratigraphic section was relatively unlithified. This both allows for the entrainment of low-permeability shale into the fault zone and precludes the preservation of open fractures along the fault zone. The geologically young Gulf Coast stratigraphy is relatively unlithified at present and would therefore have been unlithified during any past or historical fault motion.

- An appropriate calibration of SGR to fault seal and permeability is available. While a specific local calibration is not available, the SGR approach was developed and calibrated within globally analogous geologic settings. To address the lack of local calibration, ExxonMobil applied a conservative scaling of SGR to seal development. A higher SGR value corresponds to better fault seal development. For example, ExxonMobil limited seal development to SGR values greater than 0.5, while published calibration expects the onset of seal development at an SGR greater than 0.2.

- The well-based stratigraphy used in the SGR calculation is representative of the stratigraphy directly adjacent to the faults under consideration. Several well logs are available within the AOR, the majority being within [redacted] of the analyzed faults under consideration. In addition to leveraging the nearest well, the stratigraphy from a selection of other local wells was used to constrain allowable ranges of near-fault stratigraphic character. Importantly, the key identified sealing intervals (UCZ, [redacted], and LCZ) are stratigraphically continuous across the region and therefore are present in all of the local wells.

- Fault architecture was interpreted to identify relevant features and accurately characterize fault throw. Available seismic data are sufficient to identify and characterize significant faults within and surrounding the AOR. ExxonMobil factored in a 25% uncertainty margin on the fault seal analysis throw to acknowledge mapping and seismic resolution uncertainties on all faults within the AOR. Faults below seismic resolution have low throw, so they do not pose a seal risk.

[redacted] Faults

The SGR analyses for the [redacted] faults are treated here together, because the top LCZ offsets and stratigraphy—and therefore the SGR results—are very similar for all three (Figure 1-23). The faults are roughly co-linear, overlap or nearly intersect, and parallel other faults in the broader system. All [redacted] faults offset the LCZ by less than 90 feet, and fault expression in the seismic disappears near the top of the [redacted]. Because the UCZ is not offset, fault seal is not a concern; however, because the injection wells are downdip of these faults, SGR analyses are important for assessing the likelihood of cross-fault baffling in the [redacted] injection interval.

The SGR analyses were performed using the following wells:

- [redacted]

Offset of the LCZ is [redacted] feet across the western fault, [redacted] feet across the central fault, and [redacted] feet across the eastern fault. Offset decreases to zero near the top of the [redacted] With such low offset, juxtaposition of dissimilar stratigraphy is minimal and little shale is entrained in the fault zone. The SGR values therefore correlate with lithology, with low SGR (<20%) across the faults in sands and high SGR (>80%) across the faults in shales. A conservative additional 25% increase in offset does not meaningfully affect SGR values. The LCZ is approximately [redacted] feet thick at this location, so low offset preserves nearly that thickness in self-juxtaposed shale with 100% SGR, suggesting little seal risk below the injection zone.

Based on the 3D seismic data, the [redacted] faults do not reach the UCZ, and do not compromise the UCZ or pose risk to the USDW. These [redacted] faults offset the LCZ but are insubstantial relative to the thickness of this unit and so do not compromise the basal seal either. The only effect these faults potentially have is as slight baffles to CO_2 and formation fluid flow updip stratigraphically, an effect that will diminish updip in the fault(s) as offset decreases. Reservoir simulations show no effect on the pressure front or CO_2 plume migration due to juxtaposition, as is common for higher displacement faults, further suggesting minimal impact by the faults on injection.

[redacted] **Fault**

Only the [redacted] fault offsets the UCZ within the AOR (Figure 1-23). Offset of seismic reflections are ambiguous and indistinct by the time the fault intersects the UCZ; [redacted]

In the broader context, the [redacted] fault is better viewed not as an individual fault, but as the western tail of a larger fault system that has yet to fully coalesce. The [redacted] faults can be viewed through the same lens but are significantly less mature and so remain smaller and more isolated—and therefore unlikely to reach the surface without continued development of the fault system. That the [redacted] fault appears to influence the footprint of the pressure front—and the other faults do not—reflects the challenge of accurately assessing throw when fault slip is near seismic resolution. Because the [redacted] fault visibly offsets the injection zone and apparently offsets the UCZ, SGR analyses are important for assessing seal risk and reservoir baffling.

Figure 1-28 presents the [redacted] fault's SGR analysis, performed using the [redacted] his is an overly conservative estimate because in the Tepetate fault zone, fault slip is thought to decrease non-linearly into the Miocene (Hanor, 1982) and because 40 feet of throw would likely be detectable at a minimum as monoclines in the seismic reflections. This amount of throw leaves the UCZ largely intact with nearly 600 feet of shale-on-shale juxtaposition with SGR >95%. Offset though the [redacted] injection intervals is essentially the same as for the [redacted] faults, with SGR largely varying with lithology. As with these faults, the LCZ is approximately 3,941 feet thick where offset by the southern fault, and so is not compromised by relatively negligible offset. The SGR of 95–100% in the UCZ and LCZ exceed the 50% threshold for effective fault seal, suggesting no risk to the USDW. The SGR tracks with lithology in the injection intervals, and given the continuity of the southern fault, it is expected that formation fluid flow may be slightly baffled or directed by this structure.

In summary, [redacted] faults within the AOR were identified and characterized (Figure 1-23). The SGR analysis for the [redacted] fault—the only fault that appears to intersect the UCZ within the AOR—indicates that fault seal is fully maintained across this interval. The [redacted] faults intersect the pressure front and the CO_2 plume, but according to this analysis do not extend shallow enough to intersect or offset the UCZ and so pose no threat to the USDW. The SGR for these faults vary with lithology and indicate the potential for minor cross-fault baffling. Although these faults are all within the AOR, their position and characteristics are such that they do not present a risk to the USDW.

1.6 Geomechanics

The information discussed in this section is from existing sources, such as publications and proprietary offset well data. Log data from existing wells around the Mockingbird Project region are used to estimate the local stress conditions, elastic moduli, and fracture gradients of the injection and confining zones. Site-specific geomechanical information is not currently available within the proposed AOR. The primary source for this information will be the proposed Mockingbird IZM No. 01 stratigraphic test well, to be drilled approximately 2 miles northwest of the proposed Mockingbird INJ No. 03.

1.6.1 Local Stress Conditions

The World Stress Map is a "global compilation of information on the crustal present-day stress field maintained since 2009 at the Helmholtz Centre Potsdam GAZ German Research Centre for Geosciences."[1] The associated website presents the compiled regional stress data, including that for the project region as shown in Figure 1-29. Based on a review of the figure, the estimated maximum horizontal stress orientation is at approximately N90°E—and approximately parallel with the Gulf Coast. Recently acquired image logs from offset well [redacted] also confirmed the interpretation. A normal faulting stress regime is also inferred based on the World Stress Map.

[1] https://www.world-stress-map.org/

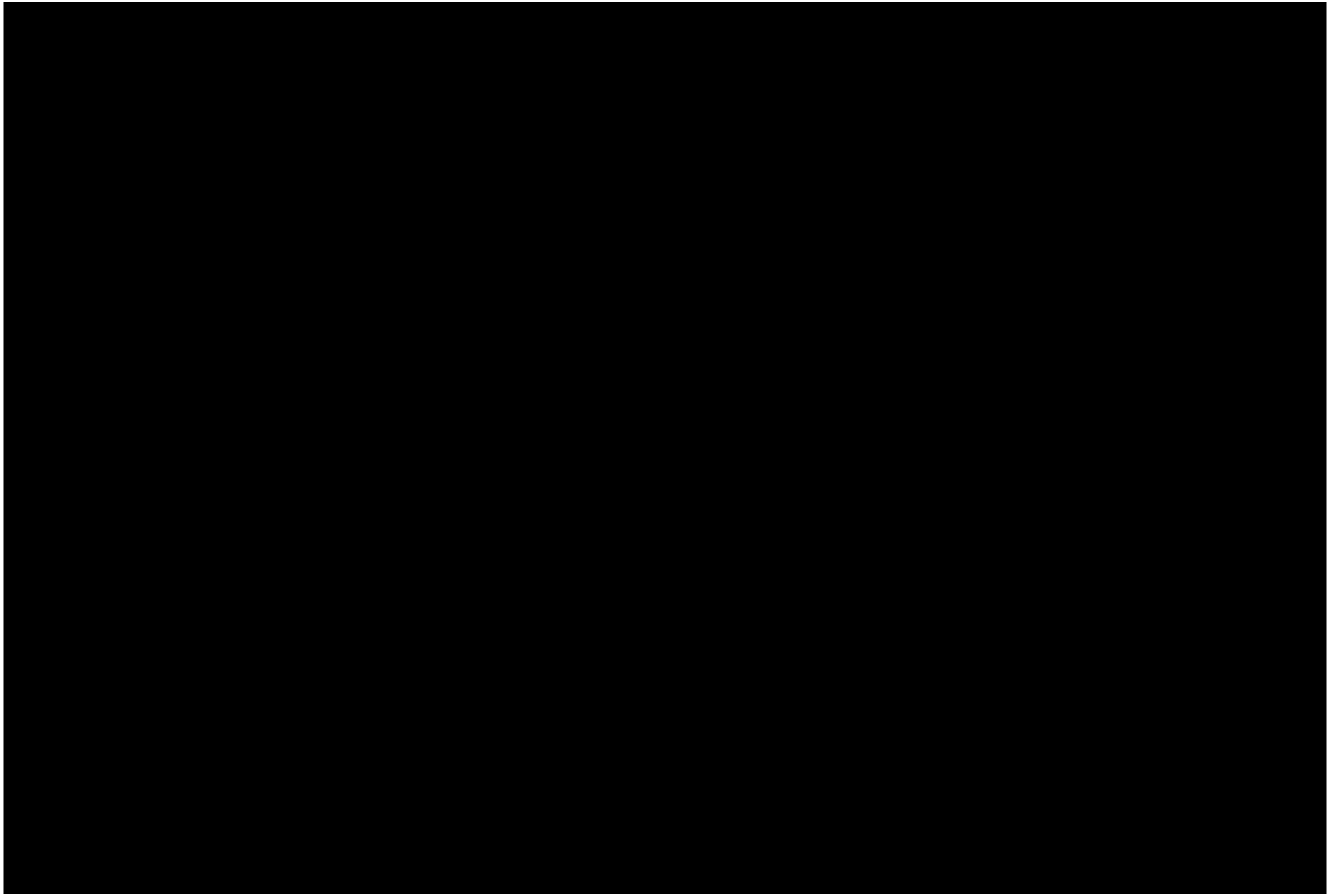

1.6.1.1 Vertical Stress

Vertical stress was characterized primarily using bulk density logs from offset wells—which Figure 1-30 shows near or in the project region—together with the density log of [redacted] The figure indicates that formation bulk density in the area follows a similar trend, which can be approximated with an exponential fit. Integrating the density log derived with the exponential fit yields the overburden stress profile shown in Figure 1-30, which gives an average gradient of 0.93 pounds per square inch per foot (psi/ft).

[redacted]

1.6.1.2 Minimum Horizontal Stress

The minimum horizontal stress, utilized to estimate the fracture gradient, was calculated in two steps: (1) calculating a Poisson's ratio using available dipole sonic log data; and (2) using Eaton's equation to estimate the minimum horizontal stress and calibrate with available measurements. Dipole sonic log data have been collected in legacy well in Evangeline Parish, Crowell Rd U Wx Ra – 6 (SN: 233104, API 170392044500, where the compressional slowness (t_p) and shear slowness (t_s) log data are used in Equation 6 to calculate Poisson's ratio (ν):

(Eq. 6)

$$\nu = \frac{0.5\left(\frac{t_s}{t_p}\right)^2 - 1}{\left(\frac{t_s}{t_p}\right)^2 - 1}$$

Using the input parameters in Table 1-6 and Equation 6 at a depth of [redacted] feet measured depth (MD) within the [redacted] sand, the resulting Poisson's ratio is [redacted]

[redacted]

Minimum horizontal stress is calculated using Eaton's equation, shown in Equation 7 where v is Poisson's ratio, S_V is the vertical stress, P_p is the pore pressure (approximately 0.45 psi/ft for the Gulf Coast), while parameter C is a constant for calibration (tectonic stress) with available data.

(Eq. 7)

$$S_{hmin} = \frac{v}{1-v}\left(S_V - P_p\right) + P_p + C$$

Input parameters, shown in Table 1-7, were used in Equation 7 at a depth of [redacted] MD within the [redacted]. The resulting minimum horizontal stress using the values in Table 1-7 is equal to [redacted]

[redacted]

The result of these calculations shows the average best estimate, within the relevant formations, of the minimum horizontal stress for the selected well to be [redacted] with depth-dependent variations along the well, shown in Figure 1-31. Log data in this figure presents the sonic curves, the calculated Poisson's ratio curve, and the resulting minimum horizontal stress curve and its gradient.

1.6.2 Elastic Moduli

Assuming that rock properties are isotropic, the dynamic Young's modulus (E_{dyn}) can be calculated using shear wave velocity and the Poisson's ratio (ν) as follows in Equation 8.

(Eq. 8)

$$E_{dyn} = 2\rho V_s^2(1+\nu)$$

where ρ is rock density and V_s is the shear wave velocity. As an example, the following input parameters (Table 1-8) were used in Equation 8 at a depth of [redacted] and gave a dynamic Young's modulus of [redacted] gigapascals (GPa), or [redacted] million psi (MMpsi).

[redacted]

A linear dynamic-to-static transform was used to convert dynamic Young's modulus into static Young's modulus (E_{sta}) as shown in Equation 9.

(Eq. 9)

$$E_{sta} = \mathrm{k}E_{dyn}$$

where *k* is a simple scaling factor and assumed to be 0.70 based on a lab test performed on representative core samples. An example of the workflow utilizing density and sonic logs to calculate Poisson's ratio and the Young's modulus is shown in Figure 1-32. The average Young's moduli in the proposed injection intervals are summarized in Table 1-9. Note that the density correlation defined in Figure 1-30 was used in the calculation, as no well in the area had both bulk density and dipole sonic log data over all of the injection intervals.

[redacted]

[redacted]

1.6.3 Fracture Gradient

1.6.3.1 Injection Zone

As discussed previously, Eaton's equation was used—with a pore pressure gradient of 0.45 psi/ft, to estimate the minimum horizontal stress in both sand and shale—and guided the estimate of the injection-zone fracture gradient. For conservatism, the lower bound of minimum horizontal stress gradient over a sand interval is chosen to represent the fracture gradient of the entire zone. The interpreted fracture gradients are shown in Table 1-10.

[redacted]

1.6.3.2 Confining Zone

Similarly, fracture gradients in the confining zone can also be evaluated. The calculated average values are shown in Table 1-11.

[redacted]

1.6.3.3 Maximum Injection Pressure Calculation

The maximum bottomhole injection pressure must not exceed 90% of the fracture pressure of the injection zone, to reduce the potential for existing fractures to propagate during normal operations. Using the estimated fracture gradient in Table 1-10, the maximum bottomhole injection pressures for the injection wells (*Section 2 – Plume Model*), at the top of each perforated interval, are shown in Table 1-12. Note that these estimates may be revised based on site data and updated well locations.

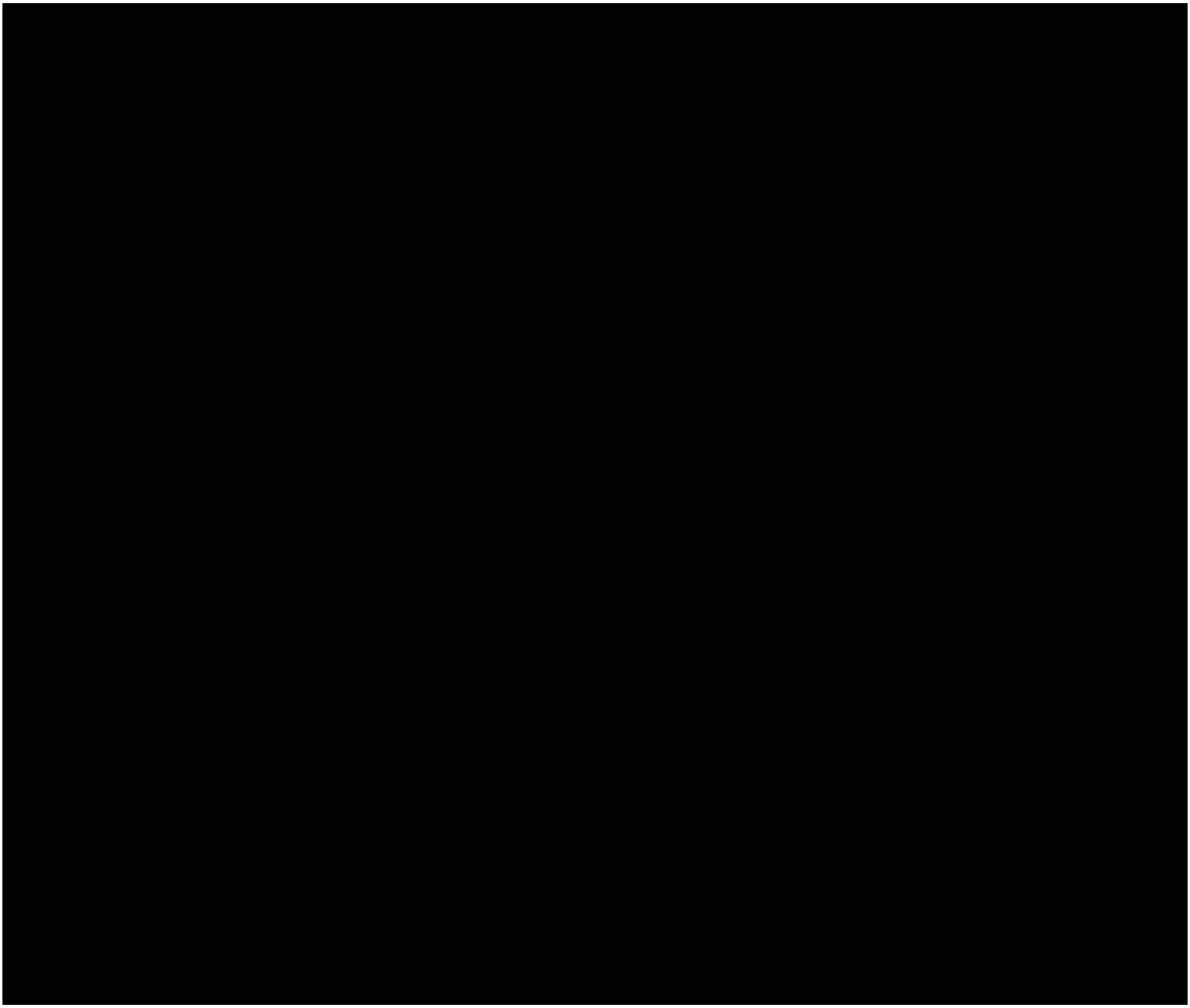

1.7 Baseline Geochemistry

Currently, there is no existing public geochemical data within the AOR. The proposed Mockingbird IZM No. 01 stratigraphic well will be used to collect geochemical and mineralogical data from key downhole units, and core tests will determine whether there is any interaction with the injectate. *Appendix B-3* presents a series of geochemical modeling completed with preexisting data to provide predictions on the compatibility of the injection intervals and sealing intervals in the AOR, with the injection of CO_2 and the subsequent CO_2-saturated brine. Geochemical precipitation and dissolution of minerals between the injected fluids and the siliciclastic [redacted] are predicted to occur at a magnitude that does not alter the volume of the minerals significantly (*Appendix B-3*).

Preexisting fluid data was taken from the U.S. Geological Survey (USGS) National Produced Waters Geochemical Database (Blondes et al., 2023). The most proximal public fluid samples from the [redacted] injection interval are within approximately 23 miles southeast of the AOR in Allen Parish and Jefferson Davis Parish (Figure 1-33). Fluid samples from these wells have the average brine properties listed in Table 1-13.

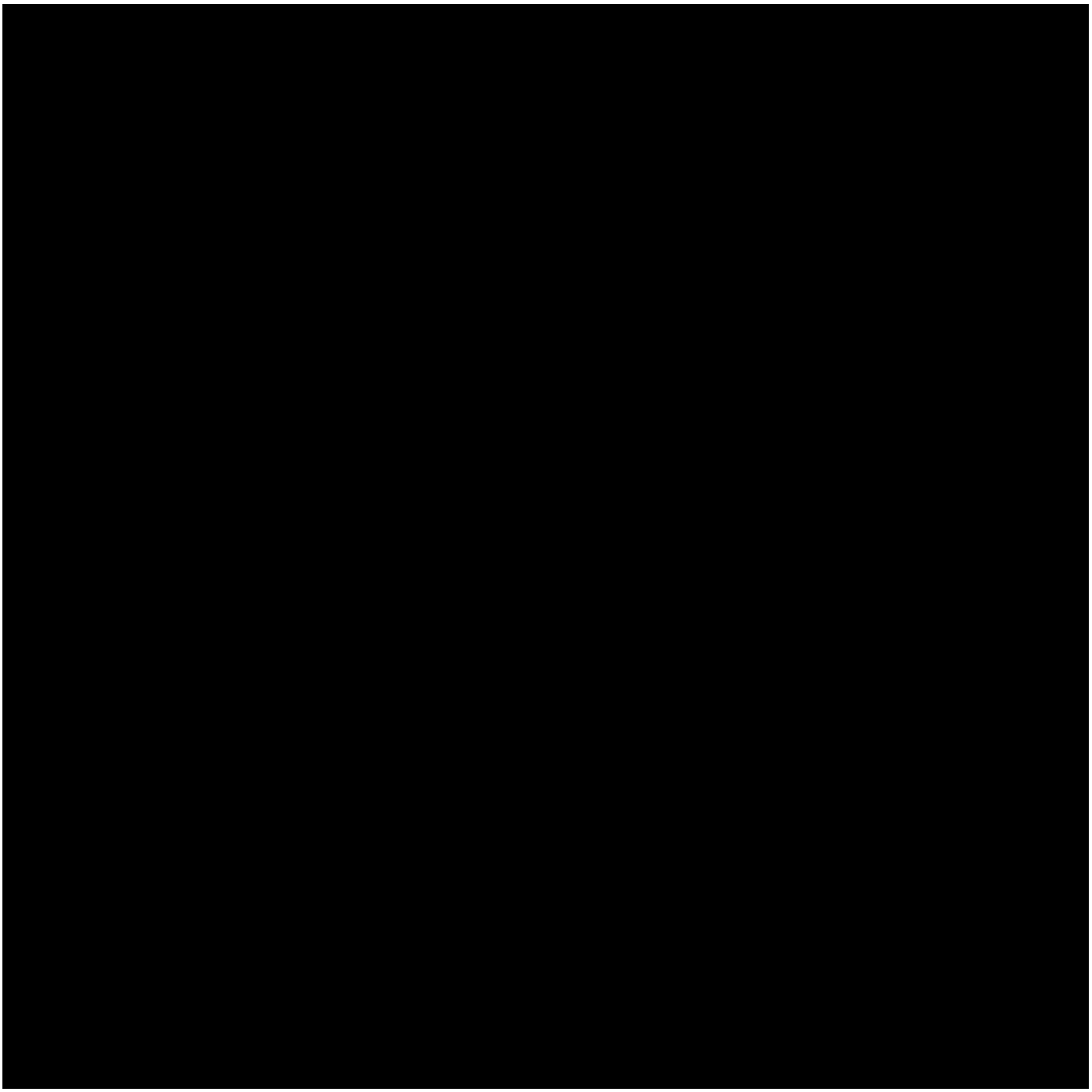

1.8 Hydrology

The following hydrologic review of Allen Parish was conducted for the Mockingbird Project to properly characterize and protect potential water resources in the state of Louisiana. The study reviewed publicly available material published by the LDENR Strategic Online Natural Resources Information System (SONRIS), the USGS, and literature from peer-reviewed journals. The LDENR and SONRIS online databases supplied helpful documents regarding water well and groundwater information. Studies released by the USGS also contributed to the hydrologic evaluation and were utilized to source figures included in this section.

1.8.1 Water Resources of Allen Parish

Allen Parish is located in southwestern Louisiana and covers an area of approximately 766 square miles (Figure 1-34). The average water withdrawal from Allen Parish in 2005 was approximately 29.2 million gallons per day (Mgal/D), sourced from both groundwater (26.75 Mgal/D) and surface water resources (2.45 Mgal/D). The Chicot, Evangeline, and Jasper aquifer systems represent the primary sources of fresh groundwater potential in the parish—for rice irrigation, public supply, aquaculture, rural domestic, general irrigation, industrial, and livestock uses. The Chicot and Evangeline aquifer systems contain freshwater throughout Allen Parish, whereas the deeper Jasper aquifer system tends to only contain freshwater in the northwestern portion of the parish. Surface water contributions within the parish occur from the Calcasieu River (2.10 Mgal/D), Bayou Blue (0.33 Mgal/D), and other miscellaneous streams (0.02 Mgal/D) (Prakken, Griffith, and Fendick, 2012).

The stratigraphic column displayed in Figure 1-35 clarifies local and regional stratigraphic nomenclatures of freshwater-bearing aquifers in southwestern Louisiana. The schematic cross sections provided in Figures 1-36 and 1-37 clarify the structural and stratigraphic relationships of these formations through southwestern Louisiana and Allen Parish.

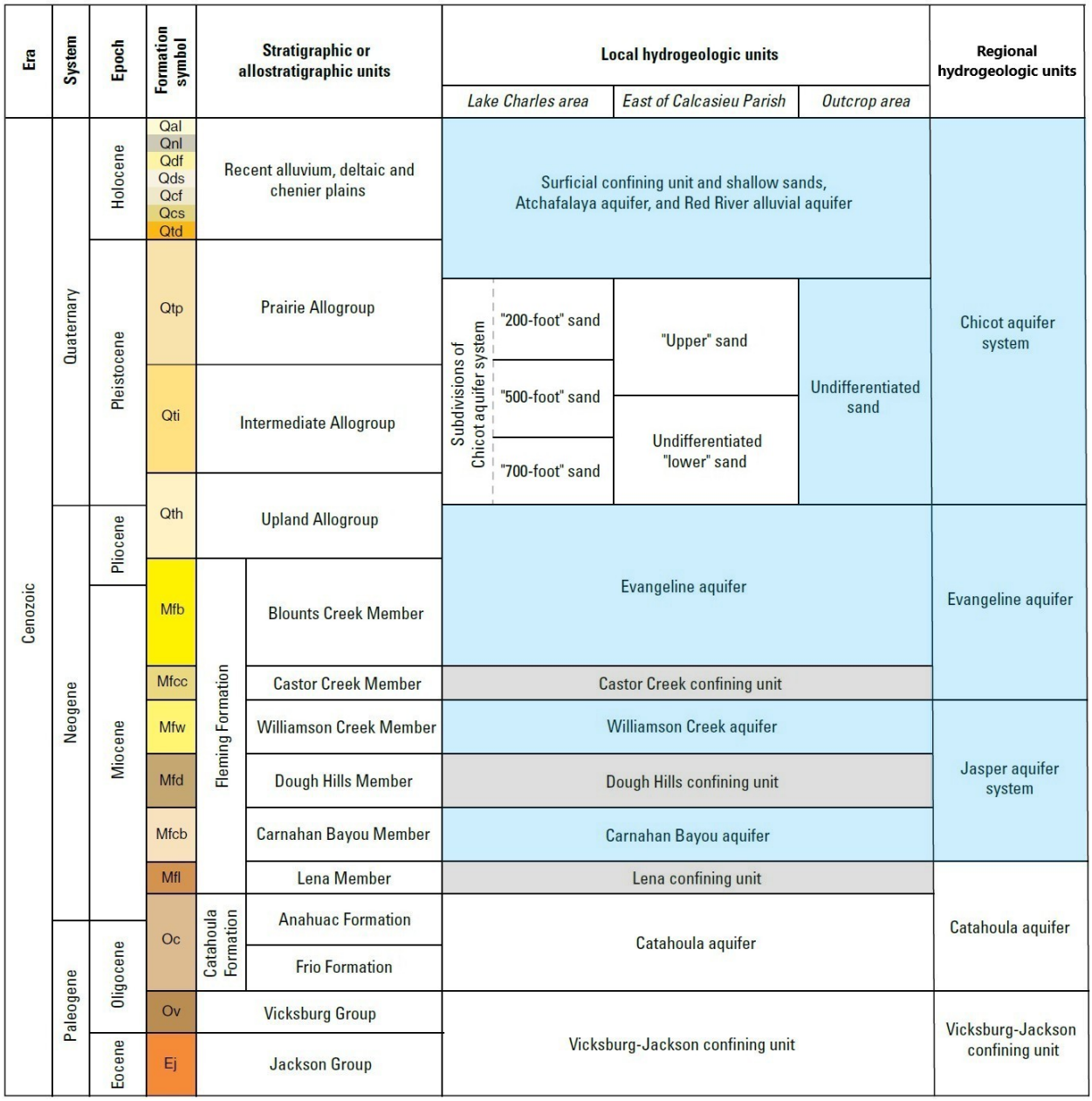

Figure 1-35 – Stratigraphic column of southwestern Louisiana with regional and local hydrogeologic units (modified from Lindaman, 2023). Formations with freshwater potential in Allen Parish are signified with blue shading.

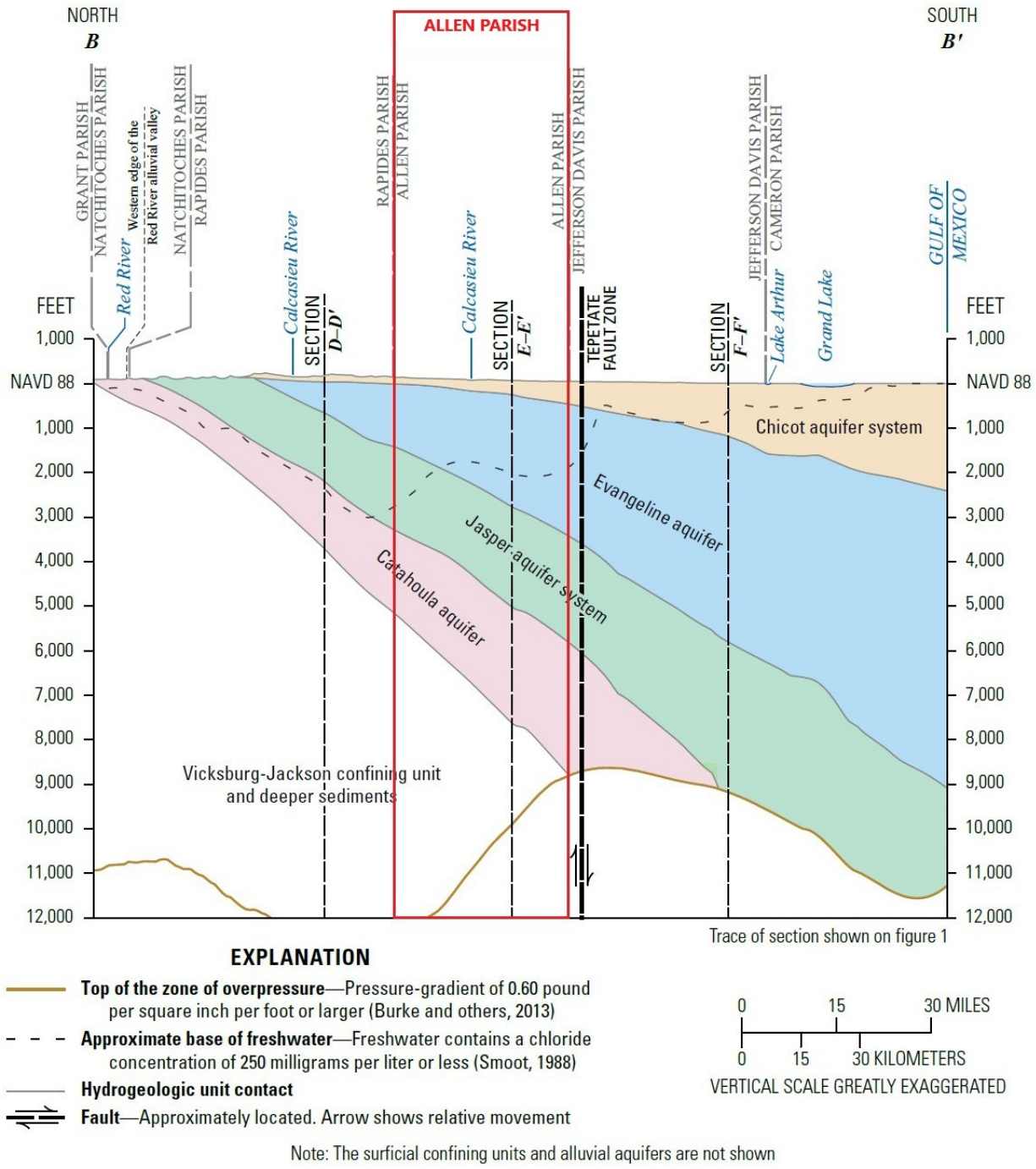

Figure 1-36 – Schematic north-to-south hydrogeologic section (B-B') through southwestern Louisiana (modified from Lindaman, 2023), with the red line clarifying the section in Figure 1-34.

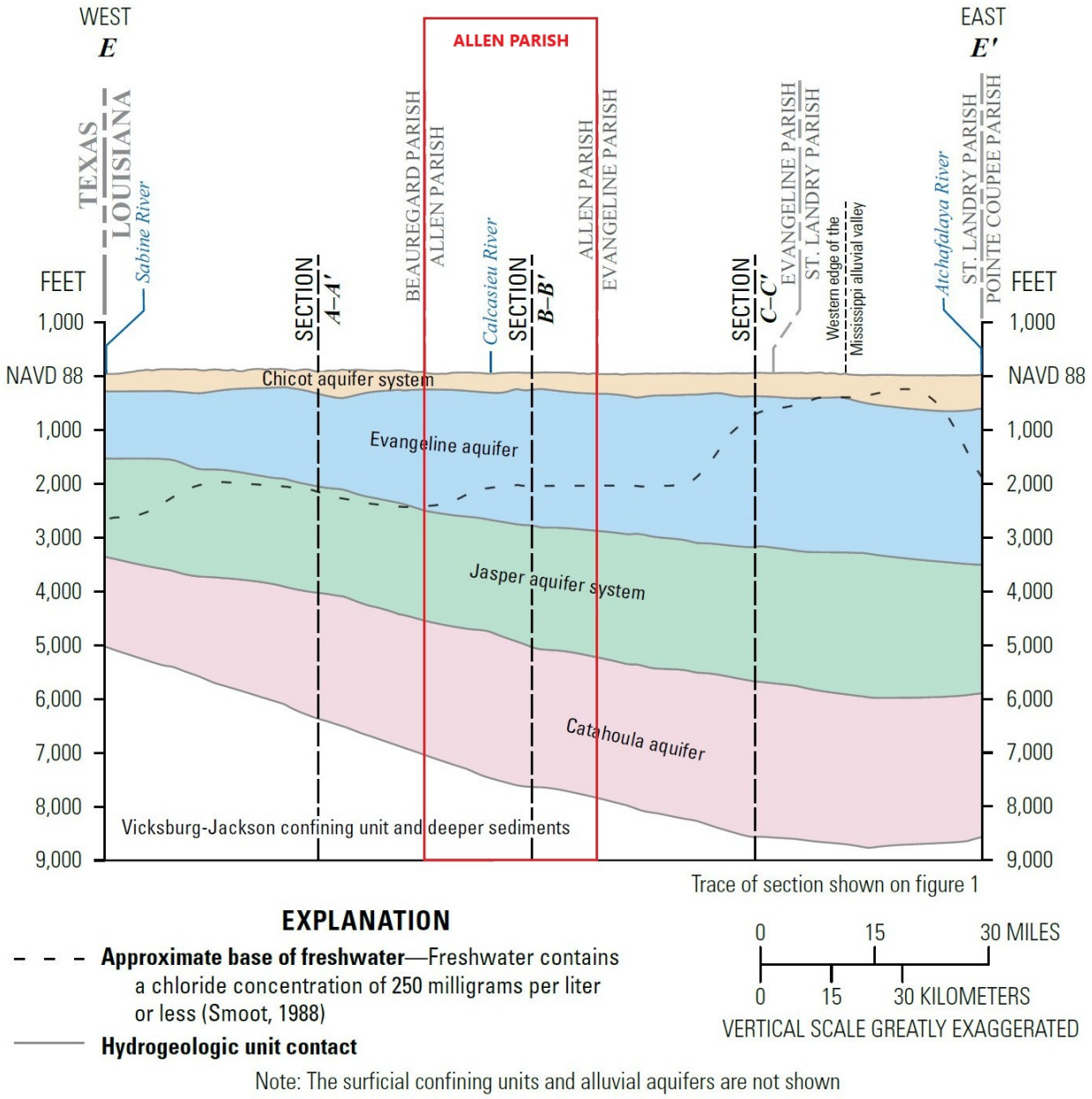

Figure 1-37 – Schematic west-to-east hydrogeologic section (E-E') through southwestern Louisiana (modified from Lindaman, 2023), with the red line clarifying the section in Figure 1-34.

1.8.2 Chicot Aquifer System

The Chicot aquifer system consists of a series of shallow Pleistocene deposits that span more than 9,000 square miles across southwestern Louisiana into portions of the Texas coastal lowlands. Aquifers are present within silt, sand, and gravel deposits interbedded with clay and sandy clay that dip and thicken toward the Gulf of Mexico (Figures 1-38 and 1-39). Moving south, deposits tend to grade from coarse sand and gravel to finer sediments that are increasingly

subdivided by clay intervals (Lovelace et al., 2002). In Allen Parish, the Chicot aquifer system is comprised of an undifferentiated sand interval overlain by a surficial confining unit of sand, silt, and clay (Prakken et al., 2012).

Shallow Sand Deposits

Shallow sand deposits occur as discontinuous sand streaks, lenses, and layers within the surficial clay confining unit. Gross thickness of the surficial confining unit typically ranges between 40–80 feet in the parish but can thin to less than 40 feet in some areas. According to the USGS Water Resources of Allen Parish report (2012), there were 75 active water wells screened in the shallow sand in 2010. Reported water well depths ranged from 13–100 feet below land surface and total water withdrawals averaged 0.09 Mgal/D (Prakken et al., 2012).

Undifferentiated Sand Interval

The undifferentiated sand interval underlies the surficial confining unit and generally consists of discrete interbeds of clay, silt, sand, and gravel. Sand deposits are typically massive and tend to fine upward through the section, from coarse sand and gravel to fine sand; these deposits can reach up to several hundred feet thick. The base of the undifferentiated sand in Allen Parish ranges from 0 feet in the north to approximately 400–500 feet below the North American Vertical Datum of 1988 (NAVD 88) in southern portions of the parish (Figure 1-38). The undifferentiated sand is present throughout the parish and supplies the majority of freshwater from the Chicot aquifer. According to the USGS Water Resources of Allen Parish (2012), there were 443 active water wells screened in the undifferentiated sand in 2010. Reported water well depths ranged from 16–450 feet below land surface with a median depth of 130 feet. Reported yields from the undifferentiated sand varied from 10–7,000 gallons per minute (gal/min) with a total average water withdrawal of 23.0 Mgal/D (Prakken et al., 2012).

1.8.3 Characteristics of the Chicot Aquifer System

Recharge and Discharge

The primary source of recharge to the Chicot aquifer system in Allen Parish is from direct infiltration of precipitation where the aquifer outcrops in Allen, Beauregard, Rapides, and Veron Parishes. Secondary recharge to the aquifer is supplied from vertical leakage through surrounding clays and natural flow from rivers and streams. Discharge from aquifers in Allen Parish generally occurs from water well withdrawals, surface flow into rivers, and communication with underlying aquifers (Prakken et al., 2012).

Potentiometric Surface and Groundwater Flow Direction

Groundwater tends to move within aquifers from areas of higher hydraulic head to areas of lower hydraulic head and the flow direction is generally perpendicular to potentiometric surface contours. A potentiometric surface map of the Chicot aquifer system published by the USGS is

provided in Figure 1-40. The map demonstrates that groundwater should flow from northwest to southeast within the project area, in agreement with interpretations published by Prakken et al. (2012).

Water Quality

Table 1-14 displays a statistical summary of water-quality characteristics from the USGS Water Resources of Allen Parish (2012). The study sourced data from 81 wells screened in the undifferentiated sand interval of the Chicot aquifer system in Allen Parish between 1940 and 2008. Water from the undifferentiated sand is generally soft, with a calcium carbonate content below 60 milligrams per liter (mg/L). Median concentrations of manganese are 55 micrograms per liter (µg/L) and generally exceed the EPA's secondary maximum contaminant levels (SMCLs) of 50 µg/L for drinking water. Median iron concentrations are 200 µg/L but exceed the SMCL of 300 µg/L in some portions of Allen Parish. The median pH is 6.2, slightly more acidic than the SMCL suggested range of 6.5–8.5 (Prakken et al., 2012).

Table 1-14 – Water-quality characteristics of freshwater from the Chicot aquifer system (undifferentiated sand) and Evangeline aquifer system in Allen Parish (Prakken et al., 2012).

	Temperature (°C)	Color, (PCU)	Specific conductance, field (µS/cm at 25°C)	pH, field (SU)	Hardness (as $CaCO_3$)	Chloride, filtered (as Cl)	Iron, filtered (µg/L as Fe)	Manganese, filtered (µg/L as Mn)	Dissolved solids, filtered
Chicot aquifer system (undifferentiated sand), 1940–2008 (81 wells)									
Median	20.7	5	151	6.2	30	18	200	55	120
10th percentile	20.0	0	62	5.3	6	5.5	<10	<1	46
90th percentile	21.5	28	271	7.9	73	32	6,700	540	206
Number of samples	51	13	55	44	59	80	31	28	40
Percentage of samples that do not exceed SMCLs	NA	77	NA	41	NA	100	55	50	100
Evangeline aquifer, 1946–95 (44 wells)									
Median	23.5	10	321	8.2	5	8.0	230	20	230
10th percentile	21.5	5	255	7.2	2	4.8	50	0	193
90th percentile	25.0	140	764	8.6	26	25	870	76	494
Number of samples	33	41	42	43	43	44	41	33	40
Percentage of samples that do not exceed SMCLs	NA	59	NA	84	NA	100	61	85	90
SMCLs									
	NA	15	NA	6.5–8.5	NA	250	300	50	500

[Values are in milligrams per liter, except as noted. °C, degrees Celsius; PCU, platinum cobalt units; µS/cm, microsiemens per centimeter; SU, standard units; $CaCO_3$, calcium carbonate; µg/L, micrograms per liter; <, less than; NA, not applicable; SMCL, Secondary Maximum Contaminant Level established by the U.S. Environmental Protection Agency (2011)]

1.8.4 Evangeline Aquifer System

The Evangeline aquifer system underlies the Chicot aquifer system and is composed primarily of fine- to medium-grained sand with interbeds of silt, clay, and localized coarse sand lenses. Permeable sand deposits of the aquifer system tend to be separated by extensive confining clay intervals that can restrict communication (Prakken et al., 2012). Sands encased within upper portions of the system are saturated with freshwater, while lower sand beds tend to be saturated with brackish to saline water (Angel and Whiteman, 1985). This is illustrated by the base of freshwater contact displayed on the regional cross section provided in Figure 1-36.

The base of the Evangeline aquifer system ranges from approximately 1,500 feet below NAVD 88 in northern Allen Parish to approximately 3,500 feet below NAVD 88 in southern portions of the parish, as illustrated on the structure map in Figure 1-41. Gross thickness of the aquifer system ranges from approximately 1,500–3,000 feet in the parish, thickening toward the south-southeast (Figure 1-42) (Lindaman, 2023). Sands bearing freshwater have an aggregate thickness of approximately 1,000 feet in central-western Allen Parish and thin to approximately 200 feet along the southern parish line. The aquifer is present throughout the parish and provides approximately 13.7% of groundwater to the parish, with the remainder supplied by the Chicot aquifer system. According to the USGS Water Resources of Allen Parish (2012), there were 34

active water wells screened in the Evangline aquifer system in 2010. Reported water well depths ranged from 390–1,720 feet below land surface with a median depth of 749 feet. Reported yields from the undifferentiated sand varied from 9–1,000 gal/min with a total average water withdrawal of 3.68 Mgal/D (Prakken et al., 2012).

1.8.5 Characteristics of the Evangeline Aquifer System

Recharge and Discharge

Recharge from aquifers in Allen Parish generally occurs from precipitation, hydraulic communication with overlying aquifers, and season inflow from rivers. Discharge from aquifers in Allen Parish generally occurs from water well withdrawals, surface flow into rivers, and communication with underlying aquifers (Prakken et al., 2012).

Base of Freshwater

Figure 1-43 portrays a structure map of the base of fresh groundwater across Allen Parish with a red star signifying the approximate location of the Mockingbird Project area. The base of fresh groundwater contact varies within Allen Parish and acts independent of aquifer systems but generally ranges between 1,500–3,500 feet below the National Geodetic Vertical Datum of 1929 (NGVD 29) (Prakken et al., 2012). The base of freshwater occurs most often within the Evangeline aquifer system—except in northern Allen Parish, where present within the Jasper aquifer system. This is illustrated by the base of freshwater contact displayed on the regional cross section provided in Figure 1-36. [redacted] The reported base of USDW depths range between 2,680–3,190 measured depth feet and are consistent with the structure map provided in Figure 1-41 and associated base of freshwater depths reported by Prakken et al., (2012).

Potentiometric Surface and Groundwater Flow Direction

Groundwater tends to move within aquifers from areas of higher hydraulic head to areas of lower hydraulic head with a general flow direction perpendicular to potentiometric surface contours. A potentiometric surface map of the Evangeline equivalent aquifer system published by the USGS is provided in Figure 1-44. The map demonstrates that groundwater has a general flow direction to the south-southeast within the project area, in agreement with interpretations published by Prakken et al., (2012).

Water Quality

A statistical summary of water-quality characteristics from the USGS Water Resources of Allen Parish (2012) was provided in Table 1-14. The study sourced data from 44 wells screened in the Evangeline aquifer system in Allen Parish between 1946 and 1995. Water sampled from freshwater portions of the aquifer is generally soft and within SMCL tolerances for drinking water.

Concentrations of iron and manganese slightly exceed suggested SMCLs within select portions of Allen Parish (Prakken et al., 2012).

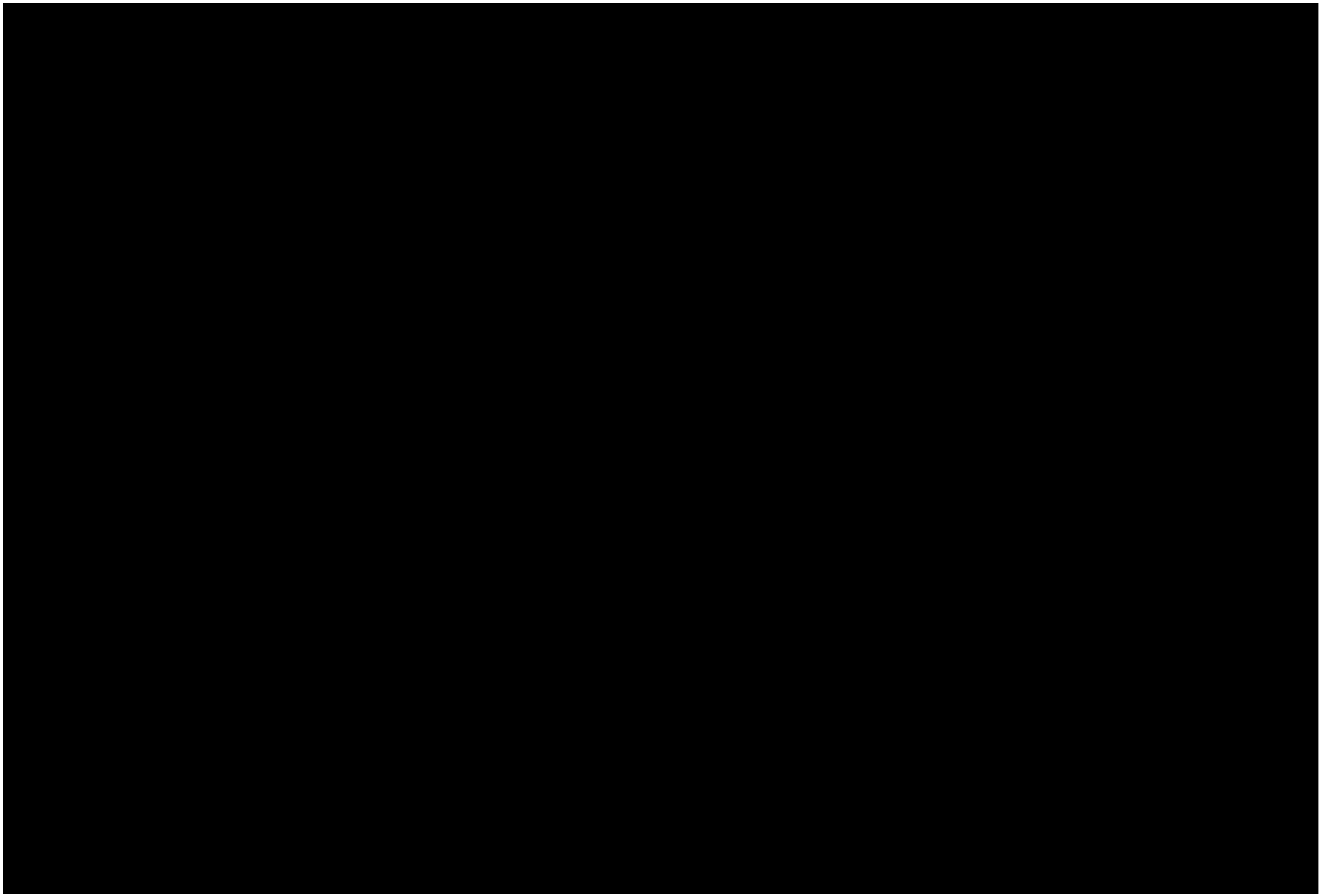

1.8.6 Jasper Aquifer System

The Jasper aquifer system is present throughout Allen Parish but only contains freshwater in northwestern portions of the parish. Downdip, in the vicinity of the AOR, the Jasper aquifer system is equivalent to the [redacted] and is a recognized saline aquifer and hydrocarbon-bearing reservoir. The base of freshwater becomes progressively shallower moving southeast in Allen Parish, while regional dip continues to deepen and aggregate thickness of freshwater sands to thin. As a result, there is a limited window of freshwater potential in the aquifer system. According to the USGS Water Resources of Allen Parish (2012), there were no active water wells screened in the Jasper in 2010. Water sampled from test holes drilled in freshwater-bearing areas of the Williamson Creek aquifer in Allen Parish suggest that the water is soft but exhibits an alkaline pH over 8.0 and iron concentrations that exceed the SMCL of 300 µg/L (Prakken et al., 2012).

1.8.7 Base of USDW Determination

For the Mockingbird Project, the base of the lowest USDW was determined from public data, review of offset wells, and a literature review. The lowest USDW base was determined using a resistivity log-based method outlined by the LDENR. This method uses the deep induction curve of the electric log along with depth and resistivity cutoffs to determine the lowermost USDW (Table 1-15). The USDW base is then established at the base of the sand unit containing the lowermost USDW, if at least 100 feet of net shale exists between the USDW base and the next zone.

Table 1-15 – Depth and Resistivity Cutoffs for USDW Consideration

Depth (f)	Resistivity (ohm-meters)
0–1,000	3
1,000–2,000	2.5
2,000+	2

In the vicinity of the Mockingbird Project, the base of the USDW is contained within the Chicot and Evangeline aquifers (Figure 1-41; Lindaman, 2023).

A subset of 30 state USDW picks were obtained from SONRIS and gridded into a base USDW surface (Figure 1-45a), with an average base USDW depth of to 2,660 feet TVDSS within the AOR. The SONRIS data set was complemented by an independent ExxonMobil assessment of USDW depth using SP and resistivity logs from 99 offset legacy wells. The USDW depths were picked using the LDENR log-based method (Table 1-15) and were gridded using the same parameters as the SONRIS USDW map (Figure 1-45b). Based on these measurements, the average USDW depth is 2,640 feet TVDSS within the project AOR. In specific wells with SONRIS picks, the ExxonMobil USDW picks are, in most cases, identical or within a few feet (Figure 1-44). While both data sets provide essentially the same result, the ExxonMobil USDW data set was used for simulation

because it is based on more than twice as many measurements (*Section 3 – Area of Review and Corrective Action Plan*).

1.9 Site Evaluation of Mineral Resources

1.9.1 Active Mining Near the Proposed Injection Location

By referencing the USGS Mines and Quarries geodatabase, nearby mineral deposits were reviewed and mapped. A sand pit to the southwest of the AOR is the closest identified feature to the project. Further afield lie other gravel pits and an open pit mine/quarry in the northwest. No surface mineral impacts from the Mockingbird Project will occur at the identified pits.

A separate search using public data provided by the USGS Mineral Resources Data System was also conducted. The primary features identified during this search were the Gulf Coast salt domes. The closest of these are the [redacted], located 19.06 miles north-northeast of the project AOR. The Roanoke, Welsh, Woodlawn and Iowa salt domes are all located greater than 20 miles south of the AOR. No impacts from the Mockingbird Project are expected to occur at these locations. At [redacted] cavern operations are being performed for natural gas storage by [redacted], as well as active saltwater disposal and oil production operations.

Of the current active natural gas storage caverns at [redacted] is the oldest, having been drilled in [redacted] Several other cavern wells have been added since, and operations continue to the present day. The features described herein are depicted in Figure 1-46.

[redacted]

1.9.2 Oil and Gas Resources

The first substantial exploration efforts for oil and gas in this part of Louisiana occurred in the 1950s, although available records show some wells possessing a spud date in the 1930s. Wells tend to follow the west-to-east trend of the Gulf Coast strata in this region. This is evident in Figure 1-47, where a couple of banks of wells in the area migrate linearly north and south of the Mockingbird Project AOR. Within 6 miles of the centroid of the AOR, [redacted] wells were drilled. Of those wells, [redacted] have recorded production data (*Appendix B-4*).

[redacted] No wells from this field lie within the modeled areal extent of the injected CO_2 plume. All wells within the AOR are plugged and abandoned, leaving offset production unaffected.

It first produced in 1959 from the Cockfield reservoir within the Northwest Oberlin field, with a perforated interval from 9,240' – 9,246', below the proposed Mockingbird Project injection interval. It produced until 2014, primarily gas, with cumulative production totaling 2,636,064 mcf. This well is outside the modeled extent of the CO_2 plume. Only two wells with historical production are located within the AOR, both produced from deeper intervals than the Mockingbird Project perforated zone of approximately 5,100 - 7,400 ft. This makes the area well suited for the injection and sequestration of CO_2. Any wellbores within the AOR that are drilled through the injection zone are discussed in *Section 3 – Area of Review and Corrective Action Plan*.

1.10 Seismic History

1.10.1 Historical Seismic Events

1.10.1.1 Seismic Monitoring Stations in and Around Louisiana from All Relevant Databases

Multiple networks of seismic monitoring stations are deployed in and around Louisiana or have been deployed in the past for earthquake and microseismic monitoring, for research, by hobbyists, and for public use (Figure 1-48). Each network has dedicated webpages to share information; however, the Incorporated Research Institutions for Seismology (IRIS) consortium maintains a website compiling information from all networks.[2]

- The U.S. National Network consists of more than 100 currently active permanent stations located in approximately 186 mile-spacing across the United States. The two closest stations are in Nacogdoches, Texas (US_NATX) and in Vicksburg, Mississippi (US_VBMS).[3]
- The Transportable Array is a network of seismometers that have operated at temporary sites across the United States. The array's deployment covered Louisiana in 2011 and 2012, with the closest seismometer in DeRidder, Louisiana, 16 miles from the Mockingbird Project. This station (TA_441A) was active from February 11, 2011, to December 06, 2012.[4] However, this station was selected to become permanent as part of the Central and Eastern U.S. network and returned to monitoring January 15, 2015 (discussed below).
- The Central and Eastern U.S. network of seismometers had one-quarter of its stations initially operating within the Transportable Array Network and then selected to become permanent. The next closest station to the Mockingbird Project after DeRidder is in Pineville, 24 miles east (N4 342B).[5]
- The Texas Seismology Network has 29 permanent seismometer stations and additional portable stations deployed throughout Texas. The station nearest to the Mockingbird Project is 100 miles away, in San Augustine (Station TX SNAG).[6]
- The Arkansas Seismic Network is a network of permanent and temporary stations operated by the Arkansas Geological Survey. The station nearest to the Mockingbird Project is 164 miles away, near Junction City, Arkansas (Station AG XA01).[7]
- The U.S. Geological Survey Network of stations is operated by the USGS Albuquerque Seismology Laboratory. The station nearest to the Mockingbird Project is 130 miles away, near Timpson, Texas (Station GS EXT05).[8]

[2] https://ds.iris.edu/ds/
[3] http://www.usarray.org/researchers/obs/reference
[4] https://earthquake.usgs.gov/monitoring/operations/network.php?virtual_network=ANSS
[5] http://www.fdsn.org/networks/detail/N4/
[6] https://www.beg.utexas.edu/texnet-cisr/texnet/earthquake-catalog
[7] https://www.fdsn.org/networks/detail/AG/
[8] https://www.usgs.gov/centers/geologic-hazards-science-center/albuquerque-seismological-laboratory

- The Global Seismographic Network has 152 seismometer stations deployed worldwide for the monitoring of earthquakes. The station nearest to the Mockingbird Project is 140 miles away, in Hockley, Texas (this station is beyond the scope) (Station IU HKT).[9]
- The Induced Seismic in Louisiana Network (ISLA) was in northwest Louisiana, operated by Tulane University and active from 2019 to 2022. The station nearest to the Mockingbird Project is 95 miles away, in Pelican (Station ZY LA11).[10]
- NetQuakes is a USGS program that deploys dense networks of seismometers to urban environments. The station nearest to the Mockingbird Project is 124 miles away, in Timpson, Texas (Station NQ ETX01).[11]
- Raspberry Shake is a hobbyist "citizen scientist" network. The station nearest to the Mockingbird Project is 39 miles away, near Simpson, Louisiana (Station AM R669E).[12]

[9] https://earthquake.usgs.gov/monitoring/operations/stations/IU/HKT/
[10] https://ebinger.wp.tulane.edu/research/isla/
[11] https://earthquake.usgs.gov/monitoring/netquakes
[12] https://raspberryshake.org/

1.10.1.2 Characterization of Seismic Events

Southern Louisiana is a tectonically quiet region, with the USGS predicting the expected number of earthquakes in a 10,000-year period to be fewer than 6 events with a 2% chance in 50 years of peak ground acceleration reaching 0.04–0.06 (Figure 1-49; USGS, 2023). [redacted] (Figure 1-49). No other earthquake in the USGS database had an epicenter 50 miles or closer to the proposed AOR. The absence of historical seismicity near the Mockingbird Project and the significant distance for historical seismic events supports that the likelihood of a seismic event within the proposed AOR is low. Information about ExxonMobil's site-specific response for seismic events is presented in the Emergency and Remedial Response Plan (*Section 8*).

[redacted]

1.10.2 Regional Faults and Project Influence

Sections 1.5.2 and *1.6* discussed regional faulting and stress conditions, respectively. Faults specific to the AOR are discussed in the following section.

1.10.3 Fault Slip Model

The injection pressures will be limited to values that reduce the potential for the initiation or propagation of fractures. No induced seismicity is expected to occur under the proposed permit

conditions. The following studies were conducted to provide a site-specific technical evaluation of the seismic risk within the AOR.

The fault slip potential was assessed using a deterministic 3D approach—based on an integrated pore-pressure prediction estimate of the stress gradients and the pore pressure increase at fault-formation interfaces. The modeled output is the approximated pore pressure needed for the fault to slip at each point on the fault. The estimates of the stresses included a vertical gradient of [redacted], a maximum horizontal stress gradient calculated using a range of [redacted] an average minimum horizontal stress gradient of [redacted], and a pore pressure gradient of [redacted] The orientation of the maximum horizontal stress was taken from the World Stress Map, trending N90°E ±10° to account for slight rotations of the stresses in the AOR. The coefficient of friction used within the modeling was [redacted].

The amount of pore pressure required for fault slip is defined as the horizontal distance between the Mohr circle and the failure line. By constraining the stress state and pore pressure at each location along the fault, based on regional leak-off test data (Shmin) and the integration of the density log (Sv)—as well as the fault geometry (fault dip and fault strike)—the critical pore pressure for fault slip can be computed by assuming a friction coefficient for faults.

This methodology neglects poroelastic stresses due to the rock frame deformation and assumes that the regional stresses are representative of the stresses at the fault location. The resulting deterministic approach indicates that injection activities would have to increase pore pressures by more than [redacted] at the shallower [redacted] injection interval to induce fault slip along the southernmost fault within the AOR. The current estimate of the maximum pore pressure increase anywhere in the injection zone, based on the simulation model, is less than [redacted] indicating that the potential for induced seismic risk based on this methodology is low.

Figure 1-50 shows the estimated pore pressure increase required to induce fault slip along mapped faults within and surrounding the AOR, intersecting at the [redacted] surface. The pore pressure increase along each fault trace is below the fault slip criterion. Fault traces are represented by spheres, colored by the pressure needed to induce reactivation. The map is contoured by maximum pressure change within the [redacted] from CO_2 injection. [redacted] (*Section 2 – Plume Model*).

Figure 1-51 shows a 3D representation of fault reactivation pressure along the surfaces of each fault within and surrounding the AOR. All faults show higher reactivation pressures with depth.

1.10.4 Seismic Hazard

Combined, the national seismic assessment, the absence of historical seismicity, and the analysis described in *Section 1.10.3* suggest that the potential for induced seismicity from CO_2 injection at the project area is not a significant risk.

Based on the seismic history of the Mockingbird Project area and the conforming pore pressure calculations, the potential for induced seismicity from CO_2 injection at the project area is not a significant risk.

1.11 Conclusion

The Mockingbird Project is a suitable location for CO_2 storage operations, having favorable geologic controlling factors related to injectivity, capacity, and containment. For the Mockingbird Project, critical favorable factors include the following:

- Multi-layered above-zone confining system with a [redacted] thick UCZ and deeper redundant intraformational seals ([redacted]); all are laterally extensive and have no structural offset within the CO_2 plume.
- Storage complex is of low structural relief, [redacted] and well constrained by 2D/3D seismic data and high-confidence well ties.
- The average vertical distance separating the USDW base to the top of injection is [redacted] with the multi-layered above-zone confining system protecting the USDW.
- The injection zone is sufficiently thick, porous, and permeable to support the proposed injection operations. The LCZ provides thousands of feet of impermeable shale to contain injected fluids to the proposed injection zone.
- [redacted] faults within the AOR have been identified, characterized, and analyzed. Shale gouge ratio analysis was conducted for all [redacted] faults, and the results of this analysis suggest that the faults are sealing across the confining interval—and not anticipated to act as conduits for fluid flow out of the injection zones. No other known conduits exist.
- Geomechanical properties and local stress conditions support the proposed Mockingbird Project operations.
- Baseline geochemistry and geochemical modeling of the in situ fluid and injectate support the containment of injected fluids to the injection zone.
- Hydrologic units above the proposed injection zone are characterized and mapped. Risk to the USDW by the Mockingbird Project's operations is low.
- Proposed operations will not affect active offset mineral resources.
- The AOR is absent of historical seismicity and is a significant distance from historical seismic events, supporting the likelihood that a seismic event is improbable.
- Fault slip potential was assessed, and no induced seismicity is expected to occur under the proposed operating conditions.

Data gathered from the proposed stratigraphic test well, Mockingbird IZM No. 1, will be utilized in the verification of interpreted data and further characterization of the site-specific geology. The site geologic and hydrologic information presented herein were used to construct a 3D geomodel to simulate the plume and demonstrate the feasibility of the project (*Section 2 – Plume Model* and *Section 3 – Area of Review and Corrective Action Plan).*

1.12 References

Allen, D.E., Strazisar, B.R., Soong, Y., and Hedges, S.W. (2005). Modeling carbon dioxide sequestration in saline aquifers: Significance of elevated pressures and salinities. *Fuel Processing Technology* 86, 1569-1580.

Albuquerque Seismological Laboratory | U.S. Geological Survey. (n.d.). https://www.usgs.gov/centers/geologic-hazards-science-center/albuquerque-seismological-laboratory

Angel, M., Jr. and Whiteman, C.D., Jr. (1985). Generalized potentiometric surface of the Evangeline and equivalent aquifers in Louisiana, 1980, Water-Resources Investigations Report 84-4359, https://doi.org/10.3133/wri844359

ANSS Stations. (n.d.). https://earthquake.usgs.gov/monitoring/operations/network.php?virtual_network=ANSS

Baker, E.T., Jr. (1979). Stratigraphic and hydrogeologic framework of part of the Coastal Plain of Texas: Texas Dept. Water Resources Rept. 236, 43 p.

Best, M.G., and Grant, S.K. (1987). Oligocene and Miocene Volcanic Rocks in the Central Pioche-Marysvale Igneous Belt, Western Utah and Eastern Navada. U.S. Geological Survey Professional Paper 1433.

Bethke, C.M. (2022). Geochemical and biogeochemical reaction modeling 3rd edition. Cambridge University Press.

Bethke, C.M., Farrell, B. and Yeakel, S. (2022). The Geochemist's Workbench (Version 12.0): Reaction modeling guide. Aqueous Solutions, LLC, Champaign, Illinois.

Bird, D.E., Burke, K., Hall, S.A., and Casey, J.F. (2005). Gulf of Mexico tectonic history: hotspot tracks, crustal boundaries, and early salt distribution. *AAPG Bulletin*, Vol. 89, 311–328.

Blondes, M.S., Knierim, K.J., Croke, M.R. et al. (2023). U.S. Geological Survey National Produced Waters Geochemical Database (Version 3.0, November 2023).

Brantley, S.L. (1992). Kinetics of dissolution and precipitation – experimental and field results. In Y.K. Kharaka and A.S. Maest (eds.), *Water-Rock Interaction.* Balkema, Rotterdam, 3-6.

Bruun, B., Anaya, R., Boghici, R. et al. (2016). Texas Aquifers Study: Chapter 6, Gulf Coast Aquifers. In: Texas Aquifers Study, Groundwater Quantity, Quality, Flow, and Contributions to Surface Water: Texas Water Development Board Report.

Chowdhury, A.H., Boghici, R., and Hopkins, J. (2006). Hydrochemistry, Salinity Distribution, and Trace Constituents: Implications for Salinity Sources, Geochemical Evolution, and Flor Systems Characterization, Gulf Coast Aquifer, Texas. Chapter 5 in: Mace, R.E. et al. (eds.), Aquifers of the Gulf Coast of Texas: Texas Water Development Board Report.

Chowdhury, A.H., and Turco, M.J. (2006). Geology of the Gulf Coast Aquifer, Texas. Chapter 2 in: Mace, R.E. et al. (eds.), Aquifers of the Gulf Coast of Texas: Texas Water Development Board Report.

Davidson, S.C., and Mace, R.E. (2006). Aquifers of the Gulf Coast of Texas: An Overview. Chapter 1 in: Mace, R.E. et al. (eds.), Aquifers of the Gulf Coast of Texas: Texas Water Development Board Report.

Duan, Z., and Sun, R. (2003). An improved model calculating CO_2 solubility in pure water and aqueous NaCl solutions from 273 to 533 K and from 0 to 2000 bar. *Chemical Geology* 193, 257-271.

Earthquake & Earth Monitoring Solutions | Raspberry Shake. (n.d.). Raspberry Shake. https://raspberryshake.org/

FDSN: AG: Arkansas Seismic Network. (n.d.). https://www.fdsn.org/networks/detail/AG/

FDSN: N4: Central and Eastern U.S. Network. (n.d.). http://www.fdsn.org/networks/detail/N4/

Galloway, W.E. (2008). Depositional Evolution of the Gulf of Mexico Sedimentary Basin, in Miall, A.D. (ed.), Sedimentary Basins of the World, Vol. 5, 505-549.

Galloway, W.E., Whiteaker, T. L., and Ganey-Curry, P. (2011). History of Cenozoic North America drainage basin evolution, sediment yield, and accumulation in the Gulf of Mexico basin. *Geosphere*, Vol. 7, No. 4, 938-973.

Gaus, I. (2010). Role and impact of CO_2–rock interactions during CO_2 storage in sedimentary rocks. *International Journal of Greenhouse Gas Control* 4, 73–89.

Gherardi, F., Xu, T., and Pruess, K. (2007). Numerical modeling of self-limiting and self-enhancing caprock alteration induced by CO_2 storage in a depleted gas reservoir. *Chemical Geology* 244 (1), 103-129.

Gray, G.G., Pottorf, R.J., Yurewicz, D.A. et al. (2001). Thermal and chronological record of syn- to post- Laramide burial and exhumation, Sierra Madre Oriental, Mexico. In: Bartolini, C., Buffler, R.T., and Cantú-Chapa, A. (eds.), The Western Gulf of Mexico Basin: Tectonics, Sedimentary Basins, and Petroleum System.

Hanor, J. S. (1982). Reactivation of fault movement, Tepetate fault zone, south central Louisiana. Gulf Coast Association of Geological Societies *Transactions*, Vol. 32, 237-245.

Haq, B.U., Hardenbol, J., and Vail, P.R. (1988). Mesozoic and Cenozoic Chronostratigraphy and Cycles of Sea-Level Change. In: Wilgus, C.K. et al. (eds.), Sea-Level Changes: An Integrated Approach, SEPM Special Publication 42, 71-108.

IRIS: Data Services. (n.d.). https://ds.iris.edu/ds/

ISLA – Investigation of Seismicity in Louisiana – EES Research. (n.d.). https://ebinger.wp.tulane.edu/research/isla/

Jacques, J. M., and Clegg, H. (2002). Late Jurassic source rock distribution and quality in the Gulf of Mexico: inferences from plate tectonic modeling. Gulf Coast Association of Geological Societies Transactions, Vol. 52, 429–440.

Lindaman, M.A. (2023). Hydrogeologic framework of southwestern Louisiana: U.S. Geological Survey Scientific Investigations Report 2023–5004, 31 p., https://doi.org/10.3133/sir20235004

Lovelace, J., Fontenot, J., and Frederick, C. (2002). Louisiana Ground-Water Map No. 14, U.S. Geological Survey.

Lundstern, J.E., and Zoback, M.D. (2020). Multiscale variations of the crustal stress field throughout North America. *Nat Commun* 11, 1951 (2020). https://doi.org/10.1038/s41467-020-15841-5

Manzocchi, T., Walsh, J.J., Nell, P., and Yielding, G. (1999). Fault transmissibility multipliers for flow simulation models. *Petroleum Geoscience* Vol. 5, European Association of Geoscientists and Engineers, 53-63.

Martin, A., and Whiteman, C.D. (1985). Generalized Potentiometric Surface of the Evangeline and Equivalent Aquifers in Louisiana, 1980. USGS Water Resources Investigation Report 87-4359. https://pubs.usgs.gov/wri/1984/4359/plate-1.pdf

NetQuakes. (n.d.). https://earthquake.usgs.gov/monitoring/netquakes

Palandri, J.L., and Kharaka, Y.K. (2004). A compilation of rate parameters of water-mineral interaction kinetics for application to geochemical modeling. USGS Open File Report 2004-1068, 64 p.

Prakken, L.B., Griffith, J.M., and Fendick, R.B., Jr. (2012). Water resources of Allen Parish: U.S. Geological Survey Fact Sheet 2012–3064, 6 p., https://doi.org/10.3133/fs20123064

Raymer, L., Hunt, E. and Gardner, J.S. (1980). An Improved Sonic Transit Time-to-Porosity Transform. Proceedings of Society of Petrophysicists and Well-Log Analysts, Houston, 1-13.

Texas Seismological Network Earthquake Catalog. (n.d.). https://www.beg.utexas.edu/texnet-cisr/texnet/earthquake-catalog

Salvador, A. (1987). Late Triassic-Jurassic paleogeography and origin of Gulf of Mexico basin. *AAPG Bulletin*, Vol. 71, 419–451.

Sawyer, D.S., Buffler, R.T., and Pilger Jr., R.H. (1991). The crust under the Gulf of Mexico Basin. In: A. Salvador (ed.), The Gulf of Mexico Basin: The Geology of North America: Geological Society of America, 53–72, doi:10.1130/ DNAG-GNA-J.53s: American Association of Petroleum Geologists, Memoir 75, 159–181.

Seismic Information. (n.d.). CERI - the University of Memphis. https://www.memphis.edu/ceri/seismic/

Seismology, I.-. I. R. I. F. (n.d.). *USArray - Reference Network*. IRIS - Incorporated Research Institutions for Seismology. http://www.usarray.org/researchers/obs/reference

Shiraki, R., and Dunn, T.L. (2000). Experimental study on water–rock interactions during CO_2 flooding in the Tensleep Formation, Wyoming, USA. *Applied Geochemistry* 15, 265–279.

Sperrevik, S., Gillespie, P.A., Fisher, Q.J. et al. (2002). Empirical estimation of fault rock properties, Hydrocarbon Seal Quantification. Norwegian Petroleum Society Special Publication Vol. 11, 109-125.

Station IU HKT. (n.d.). https://earthquake.usgs.gov/monitoring/operations/stations/IU/HKT/

Strategic Online Natural Resources Information System (SONRIS) online database and GIS mapping tool; https://www.sonris.com/

Tang, Y., Hu, S., He, Y. et al. (2021). Experiment on CO_2-brine-rock interaction during CO_2 injection and storage in gas reservoirs with aquifer. *Journal of Chemical Engineering* 413, 127567.

Thorkildsen, D., and Quincy, R. (1990). Evaluation of Water Resources of Orange and Eastern Jefferson Counties, Texas: Texas Water Development Board Report 320.

U.S. Geological Survey (2023). 2023 US 50-State Long-term National Seismic Hazard Map. https://www.usgs.gov/programs/earthquake-hazards/science/2023-50-state-long-term-national-seismic-hazard-model

Warick, P.D., and Corum, M.D. (eds.) (2012). Geologic framework for the national assessment of carbon dioxide storage resources. U.S. Geological Survey Open-File Report 2012-1024.

Winker, C.D., and Buffler, R.T. (1988). Paleogeographic evolution of early deep-water Gulf of Mexico and margins, Jurassic to Middle Cretaceous (Comanchean). *AAPG Bulletin*, Vol. 72, 318–346.

Wolery, T.J. (1992). EQ3/EQ6, A software package for geochemical modeling of aqueous systems: package overview and installation guide (Version 7). Lawrence Livermore National Laboratory Report, UCRL-MA-110662, 66 p.

Xu, T., Sonnenthal, E., Spycher, N. and Pruess, K. (2006). TOUGHREACT – A simulation program for non-isothermal multiphase reactive geochemical transport in variably saturated geologic media: Applications to geothermal injectivity and CO_2 geological sequestration. *Computers & Geosciences* 32, 145-165.

Xu, T., Zhend, L., and Tian, H. (2011). Reactive transport modeling for CO_2 geological sequestration. *Journal of Petroleum Science and Engineering* 78, 765-777.

Yielding, G., Freeman, B., and Needham, D.T. (1997). Quantitative fault seal prediction, *AAPG Bulletin*, Vol. 81 (6), 897-917.

Young, S.C. et al. (2016). FINAL REPORT: Identification of Potential Brackish Groundwater Production Areas - Gulf Coast Aquifer System. Prepared by INTERA Inc. for Texas Water Development Board, Contract Report Number 1600011947.

Zerai, B., Saylor, B.Z., and Matisoff, G. (2006). Computer simulation of Co2 trapped through mineral precipitation in the Rose Run Sandstone, Ohio. *Applied Geochemistry* 21 (2), 223-240.

Appendix B – Site Characterization